2007-07-18

Development of Chemomechanical Functionalization and Nanografting on Silicon Surfaces

Michael Vernon Lee
Brigham Young University - Provo

DEVELOPMENT OF CHEMOMECHANICAL FUNCTIONALIZATION AND NANOGRAFTING ON SILICON SURFACES

by

Michael V. Lee

A dissertation submitted to the faculty of

Brigham Young University

in partial fulfillment of the requirements for the degree of

Doctor of Philosophy

Department of Chemistry and Biochemistry

Brigham Young University

August 2007

BRIGHAM YOUNG UNIVERSITY

GRADUATE COMMITTEE APPROVAL

of a dissertation submitted by

Michael V. Lee

This dissertation has been read by each member of the following graduate committee and by majority vote has been found to be satisfactory.

Date	Matthew R. Linford, Chair
Date	Adam T. Woolley
Date	Matthew C. Asplund
Date	David V. Dearden
Date	Larry L. Howell

BRIGHAM YOUNG UNIVERSITY

As chair of the candidate's graduate committee, I have read the dissertation of Michael V. Lee in its final form and have found that (1) its format, citations, and bibliographical style are consistent and acceptable and fulfill university and department style requirements; (2) its illustrative materials including figures, tables, and charts are in place; and (3) the final manuscript is satisfactory to the graduate committee and is ready for submission to the university library.

Date	Matthew R. Linford Chair, Graduate Committee

Accepted for the department

Date	David V. Dearden Graduate Coordinator

Accepted for the college

Date	Thomas W. Sederberg Associate Dean, College of Physical and Mathematical Sciences

ABSTRACT

DEVELOPMENT OF CHEMOMECHANICAL FUNCTIONALIZATION AND NANOGRAFTING ON SILICON SURFACES

Michael V. Lee

Department of Chemistry and Biochemistry

Doctor of Philosophy

Progress in chemomechanical functionalization was made by investigating the binding of molecules and surface coverage on the silicon surface, demonstrating functionalization of silicon with gases by chemomechanical means, analyzing atomic force microscopy probe tip wear in atomic force microscopy (AFM) chemomechanical nanografting, combining chemomechanical functionalization and nanografting to pattern silicon with an atomic force microscope, and extending chemomechanical nanografting to silicon dioxide. Molecular mechanics of alkenes and alkynes bound to Si(001)-2x1 as a model of chemomechanically functionalized surfaces indicated that complete coverage is energetically favorable and becomes more favorable for longer chain species. Scribing a silicon surface in the presence of ethylene and acetylene demonstrated chemomechanical functionalization with gaseous reagents, which simplifies sample cleanup and adds a range of reagents to those possible for chemomechanical functionalization. Thermal desorption spectroscopy was performed on chemomechanically functionalized samples and demonstrated the similarity in binding of molecules to the scribed silicon surface and

to the common Si(001)-2x1 and Si(111)-7x7 surfaces. The wearing of atomic force microscope probe tips during chemomechanical functionalization was investigated by correlating change over time and force with widths of created lines to illustrate the detrimental effect of tip wear on mechanically-driven nanopatterning methods. In order to have a starting surface more stable than hydrogen-terminated silicon, silicon reacted with 1-octene was used as a starting surface for AFM chemomechanical functionalization, producing chemomechanical nanografting. Chemomechanical nanografting was then demonstrated on silicon dioxide using silane molecules; the initial passivating layer reduced the tip friction on the surface to allow only partial nanografting of the silane molecules. These studies broadened the scope and understanding of chemomechanical functionalization and nanografting.

ACKNOWLEDGMENTS

in memory of my grandpa's example

for the Lord who lets me live

and for my parents who reared me to live well

Table of contents

List of figures

List of tables

Chapter 1. Introduction

Motivation

In the 1980s and 1990s, when scanning probe microscopies (SPM) were first introduced,[1,2,3,4,5] manipulating matter on an atomic scale was demonstrated and the possibilities of this advance began to take shape. Theoretically, the ability to control matter on the molecular and atomic scale should allow the creation of virtually any structure possible. Referencing biological systems as the standard, precise atomic-scale control of matter allows creation of systems that far exceed the complexity of the man-made systems manufactured today.

The feature size attainable by photolithography, the workhorse of the semiconductor industry, has been gradually scaled down to the tens of nanometers. This reduction in size of transistors and other electrical components reduces power requirements and allows more circuits to be produced in a given area. This reduction also amplifies the number of components produced on each wafer and, through the principle of economy of scale, decreases the cost of each component and increases availability in the market.

Although within two orders of magnitude of the atomic-scale, the structures and devices produced by commercial semiconductor processes are only compatible with a limited set of materials and substrates. Photolithography is optimized for a narrow range of inorganic materials, primarily semiconductors, especially silicon, and their oxides, as well as metals. The commercial semiconductor process is typically a top-down approach, which creates a pattern by removing unwanted portions of a layer rather than a bottom-up approach, where each layer is grown or formed in the desired pattern. In top-down approaches, the decrease in size comes at a cost of sensitivity to smaller defects,

specialized optical requirements, more expensive light sources, and greater precision requirements for alignment of successive masks.[6]

The versatility of organic chemistry combined with the precision of semiconductor-based technology expands the possibilities available with nanopatterning. Organic chemistry provides a broad array of building blocks, with defined reactions and structures as well as tunable properties. Organic chemical knowledge is developed by research in all chemical areas—as varied as the pharmaceutical, polymer, agricultural, and biomedical fields. The combination of organic reactions with the well-developed surface patterning technology of the semiconductor industry enables the realization of self-assembling structures to assist in microchip fabrication for the commercial lithography community,[7,8,9,10,11] in addition to inexpensive and sensitive sensors and [12,13,14,15] nanoscale bioarrays.[14,15,16,17,18,19]

Nanoscale patterning methods

There are three general approaches to nanoscale-patterning. (1) Electrically-driven approaches apply a voltage to induce changes in the substrate, a chemical in solution, or a species adhered to an SPM tip. The voltage induces an electrochemical change that leaves a pattern on the surface. (2) Diffusion-driven methods use an "inking" process, where a source, usually a polydimethylsiloxane (PDMS) stamp or an atomic force microscopy (AFM) tip, is dipped into a reservoir holding a molecule of interest and then brought into intimate contact with a substrate. The "ink" diffuses from the source at the points of contact and physisorbs or chemisorbs on the substrate. (3) Mechanically-driven methods use a mechanical force to produce a surface where the molecule of interest can

chemisorb. Typically, these methods employ the mechanical force to remove a passivating layer from the substrate or to actually alter the substrate.

Electrically-driven methods

The field of nanolithography is the crossover between the top-down patterning world of traditional lithography and the self-assembling, bottom-up world of organic chemistry. Various nanolithographic methods, most of which are SPM-based, are invaluable tools in the integration of these two worlds. The first electrically driven nanopatterning method used an STM to position xenon atoms on a copper surface.[2] One of the oldest nanopatterning methods using an AFM is based on the pioneering work of Jacob Sagiv on self-replicating, self-assembled monolayers. The use of these monolayers in nanoscale control of surface properties has been invaluable to the evolution of nanopatterning. Sagiv's work provided some of the first evidence of patterned self-assembly of nanoscale structures on surfaces based on silane layers on oxide surfaces.[20,21,22,23] When coupled with the AFM nanometer-scale resolution and the ability to apply a voltage to the tip and oxidize the monolayer in a specified pattern, this led to patterning by electrochemical oxidation.

The initial published experiments with electrochemical oxidation demonstrated that a vinyl-terminated silane layer could be oxidized to a carboxylic acid chemically or electrochemically with a voltage applied through an AFM tip. Another silane, octadecyltrichlorosilane (OTS), would then self-assemble and bind selectively on the oxidized monolayer areas.[24] This was later expanded to show that even the end $-CH_3$ group on alkyl chains can be oxidized and allow subsequent addition of silanes.[25,26,27] Succedent experiments showed that various functional groups allowed adsorption of

metal ions, allowing patterns combining semiconducting, insulating, and conducting structures.[25,28,29,30] As the research has progressed, complex patterns bridging nanoscale and micro scale structures have been produced.[26,27,28,31]

Other methods closely related to electrochemical oxidation are cathodic and anodic electrografting, electro-pen lithography, and AFM electropolymerization. Instead of electrochemically modifying a layer already on the surface, electrografting electrochemically catalyzes a reaction that binds molecules from solution to a surface to form a pattern. Cathodic electrografting (CEG) directly attaches alkynes to the surface with a single bond, whereas anodic electrografting (AEG) yields an unsaturated alkyl surface with each molecule bound by two bonds.[32,33] Electrografting can also be used to functionalize porous silicon and modify its electroluminescent properties.[34] Electro pen lithography uses a voltage applied to an AFM tip coated with silane to oxidize a thin organic film on a surface which, in turn, attracts and binds the silane molecules from the tip.[35] In AFM electropolymerization a voltage applied to an AFM tip over a conducting polymer precursor molecule deposited on a substrate causes the precursor to polymerize and form ~50 nm conducting polymer wires.[36] A further electrochemical method uses an AFM tip coated with platinum or gold ions, which, depending on the potential, can either electrochemically reduce the metal ions and deposit them on hydrogen-terminated silicon or make silicon dioxide raised features on the surface.[37,38]

Diffusion-driven or "inked" methods

Another common and well developed method that bridges to the nanoscale is microcontact printing. Microcontact printing was first introduced in 1993 by George Whitesides, *et al*.[39,40] In microcontact printing, a stamp is fabricated, most often by curing

polydimethylsiloxane (PDMS) on a silicon mold produced by commercial photolithography. The PDMS stamp is peeled off and it then bears the negative of the original mold. The stamp is inked with the desired molecule and pressed against the surface to be patterned. With the correct pressure and deposition time, only the raised areas on the PDMS stamp will contact the surface. This allows self-assembly of monolayers in the desired pattern. [41,42,43]

The procedure is quite general and useful for mass production of any pattern for which a master can be made; indeed, with specially designed masters, stamps can produce patterns with features finer and more complex than the photolithographic patterns used to create the stamps. [44] Often the patterns are used as an etch resist, as has been demonstrated with octadecyltrichlorosilane on various combinations of silicon, titanium, aluminum, nickel, and gold.[45,46,47] Microcontact printing of silanes to pattern insulating oxides of silicon, aluminum, and titanium has also been demonstrated.[48,49] Although a large amount of research has included etching in a top-down patterning approach,[45,46,47,48,49] microcontact printing has been shown to allow patterning of proteins as well as a seed layer for electroless deposition of copper.[50,51]

Dip-pen nanolithography (DPN) works on a principle similar to microcontact printing in that a molecular ink is applied to a substrate; however, in DPN the source of ink is an AFM tip. Instead of having a specific stamp, the AFM tip can draw any pattern desired. Serial patterning with the use of a single AFM tip, as opposed to a complete pattern deposition with microcontact printing, does limit the speed of patterning. However, arrays of tips have been demonstrated to feasibly amplify the speed of patterning.[43,52]

DPN has been used for a variety of molecular inks and applications. Examples of demonstrated inks are thiols on gold,[53] hexamethyldisilazane (HMDS) on SiO_2 and on GaAs,[54] and individual gold nanoparticles on mica.[55] These different inks can be interdigitated in a single pattern.[56] Like microcontact printing, the deposited inks can be used as an etch resist.[57] Patterns created by DPN have also been used for biological applications like orthogonal DNA assays,[58] as well as in studies as varied as the interactions of functionalized nanotubes with surfaces[59] and studies of kinetics of diffusion and monolayer formation.[60,61] An advantage of DPN over other methods is the recently demonstrated erasure of patterns.[62]

Mechanically-driven methods

Nanografting is a process in which an AFM tip, or any other sharp tip with a light applied force, mechanically removes a monolayer from a substrate in the presence of a molecule that will self-assemble in the place of the original layer. If repeated, this process allows multiple different molecules to be patterned on a single surface. The process evolved from experiments done with thiols on gold. Whitesides' group demonstrated that a scalpel or a carbon fiber drawn through a thiol monolayer on gold with a low applied force could displace the thiol layer with minimal disturbance to the gold.[63] When the sample was dipped into a solution of another thiol, the second thiol self-assembled onto the exposed gold. The authors suggested that this could also be done with an AFM tip. Xu and Liu expanded this suggestion and built upon previous experience with AFM tribology to develop nanografting which is simultaneous removal of a passivating layer and replacement by some molecule of interest.[64,65,66]

AFM chemomechanical functionalization is another mechanically-based nanopatterning method. Where nanografting focuses on the removal and replacement of a passivating molecule, chemomechanical functionalization focuses on priming the surface for reaction. When a surface is scratched, bonds are broken and radicals are formed that will readily react with an available functional molecule.[67] By covering a surface with a liquid with a functional group that is reactive with silicon radicals and then scratching the surface, any molecule with a silicon radical reactive functional group can be bound to and patterned on a surface.[68,69] This method has also been extended to the nanoscale.[70]

Comparison of methods

Thus far, AFM nanopatterning methods are not able to compete with photolithography in the mass production of complex, multi-layer microprocessors and computer memory. The AFM methods are many orders of magnitude slower at patterning whole wafers because of the inherent parallelism in photolithography. Bottom-up approaches, both AFM-based and microcontact printing are more amenable for applications that require low-temperature processes and especially organic layers. They can also be applied to unconventional substrates like glass and plastic, which significantly lowers cost and weight while also providing greater durability and allowing special properties like flexibility. Microcontact printing is better able to match the parallelism of photolithography than AFM-based methods and has already begun to be applied to commercial applications like organic light emitting diodes[71] and patterned magnetic storage media.[72] AFM-based methods are further from commercial development. However, massive arrays of tips and the increased push for environmentally friendly

processes, low-k dielectrics that are often organic, and smaller feature sizes move these methods closer to compatibility with desired nanofabrication processes.

As AFM-based methods become more developed and begin to penetrate commercial applications, their relative advantages and disadvantages will become more visible. The diffusion-driven processes require inking, which may significantly slow the process if the ink will not last through a complete patterning step; they also require precise timing for deposition of optimal patterns, else the pattern resolution degrades. Diffusion-driven methods, however are able to deposit molecules that chemisorb on a surface, as well as those that physisorb, making the method attractive for some biological applications. Electrically-driven and mechanically-driven methods can have the molecule for deposition present in solution or it can be added afterwards. If the molecule is present on the surface, then the surface must be passivated to prevent non-specific adsorption. This is often not a problem because the deposition is induced by applying a field or a force. AFM chemomechanical functionalization provides covalent patterning of molecules that cannot be deposited by the other methods and provides a very versatile mechanism. Any functional group that is reactive to a radical could theoretically be covalently patterned on a surface.

History and development of chemomechanical methods

Chemomechanical functionalization began with grinding silicon in the presence of alkenes and alkynes to create hydrophobic silicon particles.[67,73] Later work refined the method to allow patterning on planar silicon. Molecules terminated with a reactive group react with the silicon radicals to form a monolayer on the scribed surface. Hydrophobic alkyl layers created by chemomechanically functionalizing with long alkyl-chain 1-

alkenes provide a drastic change in free-energy compared to a clean hydrophilic silicon dioxide surface. The extent of the change was illustrated by patterning "corrals" of hydrophobic lines on a hydrophilic surface and filling the hydrophilic areas with water. Even with the surface vertically oriented, the water was confined on the surface within the corrals.[68,69] Further macroscale research showed monolayers could be formed by chemomechanical functionalization on silicon with alkenes,[68, 74] alkynes,[68] alcohols,[74] aldehydes,[75] alkyl halides,[76] epoxides,[77] and acid chlorides.[78]

Chemomechanical functionalization is based upon the simple concept that cleavage of a bond produces reactive radical species.[67] In the case of scribing silicon by chemomechanical functionalization, the crystal should preferentially cleave along the thermodynamically favored {001} and {111} silicon surfaces. These silicon surfaces that should largely represent the scribed silicon surface tend to exhibit radical character.[79] The monolayers produced by chemomechanical functionalization self-assemble into a closely packed monolayer similar to those produced by reaction of unsaturated hydrocarbons with hydrogen-terminated silicon.[80, 81, 82] These well-ordered monolayers protect the patterned surface; they have been demonstrated to be stable even in refluxing *m*-xylene[74] and boiling solutions of sulfuric acid.[83]

The radical silicon surfaces that are produced by scribing during chemomechanical functionalization will be similar if not identical to those that have been studied for decades in ultra-high vacuum (UHV) conditions. The common {001} and {111} silicon planes undergo reconstruction to produce the Si(100)-2x1 and Si(111)-7x7 surfaces, respectively, which are among the most studied surfaces in surface science.[84,85,86,87,88,89] The radical character of these surfaces suggests that Si(100)-2x1 and Si(111)-7x7 provide

good models for predicting surface characteristics, reaction mechanisms, and resulting monolayers created by chemomechanical functionalization.

The radical character of the silicon surface has been examined by both *ab initio* and semi-empirical methods. *Ab initio*, meaning from "first principles," methods are based on Schrödinger's wave equation rather than on empirical data and are generally considered to give the most accurate results. However, the computational power required limits *ab initio* calculations to small sets of atoms; these calculations are used to investigate reaction mechanisms. In order to model surface properties, which require larger ensembles of atoms, the calculations must be simplified to reduce the computation time and supplemented by empirical results to maintain some level of accuracy. One such method is molecular mechanics modeling which uses empirical results to define a "force fields" that quantify interactions between types of atoms in the model.

Ab initio results have been used to explore binding of different molecules to the silicon surface. Although other reactions may occur,[90,91,92] the binding of alkenes and alkynes to the Si(100)-2x1 surface is principally a [2+2] cycloaddition-like reaction between a Si=Si dimer on the surface and a pi bond on the unsaturated hydrocarbon.[93] This results in two Si-C σ bonds between the molecule and the surface. Acid chlorides are believed to react with the surface in a two-step process where the chlorine is abstracted by one silicon radical and the carbon radical reacts with another silicon surface radical.[78] The reaction of an alcohol molecule with a bare silicon surface is believed to occur by a surface silicon radical attacking and binding the oxygen, followed by hydrogen abstraction by another surface silicon radical to form an alkoxy-terminated surface.[86] In the case of epoxide molecules with the silicon surface, the silicon radical is believed to attack the oxygen of

the oxirane ring and form a secondary carbon radical that can either react with another silicon radical to form a five-membered ring or abstract a hydrogen atom from a neighboring molecule or a solvent molecule to form an alkoxy-terminated surface.[77]

Frequently the actual mechanism of binding is less important than the aggregate properties of the surface, which currently are too complex for computation by *ab initio* methods. Molecular mechanics modeling has been used to inspect surface coverage and packing of alkyl chains in monolayers on silicon surfaces. Some studies corroborated experimentally-derived 50% substitution percentages for alkyl monolayers on Si(111) and examined the resultant packing of the alkyl chains.[94,95] A similar investigation of the completion of monolayers and their respective packing on silicon created by chemomechanical functionalization is included in this dissertation as Chapter 2.[96]

The refinement of the chemomechanical functionalization process includes many aspects; for instance, increasing the number of reactants available for use, reducing and expanding the size of features that can be produced, improving the resolution of the features, reducing the roughness of the functionalized surface, and extending the process to other substrates. Toward these ends, work was conducted that improved control over the tip and the forces it exerts on the surface, introduced a variant on the original method allowing gaseous reagents to be used, transferred the whole process of chemomechanical functionalization to the nanoscale with an AFM, and merged AFM chemomechanical functionalization with nanografting.

One of the initial advances to chemomechanical functionalization was to use a tip made from a tungsten carbide ball or from a spherical ruby. The large radius of curvature relative to the size of the features allowed greater control over the pressure applied to the

surface. This allowed features as shallow as a couple of nanometers to be produced, which contrasts features from the original scribing tips with roughness of microns. The spherical tips with elevated hardness significantly reduced the roughness of chemomechanically functionalized surfaces.[97] Also significant was the use of a compliant mechanism to both measure and control the force applied to the chemomechanically scribing tip. This mechanism allowed forces below 200 mN to be reproducibly applied in the vertical direction while also providing better lateral stability.[98] A further advance on the macroscale was the demonstration of chemomechanical functionalization in the presence of a gaseous alkene and alkyne. This broadens the scope of reagents available for functionalizing a silicon surface in an open lab environment to include all alkenes, alkynes, alcohols, aldehydes, alkyl halides, epoxides, and acid chlorides that are gases as well as liquids. An added advantage is the elimination of the need to clean samples to remove excess reagent following functionalization. This advance is included as Chapter 3.[99]

In 2003, chemomechanical functionalization was extended to the nano- scale. Davis, *et al.*, demonstrated chemomechanical functionalization with an alkene on hydrogen-terminated silicon. The hydrogen-termination limits oxidation and allows the silicon surface to be abraded in the presence of a functional molecule before the hard, protective oxide forms. 30 nm lines were produced, comparable with other SPM techniques. A relationship was noted between applied force and the width of features created.[70] This relationship has been quantified in a tribology study.[100]

The initial demonstration left room for improvement. The stability of the hydrogen-termination is limited, so it would be advantageous to be able to use a more passive

starting surface. This was accomplished by starting with an alkyl-terminated silicon surface, effectively merging chemomechanical functionalization with nanografting into chemomechanical nanografting.[101] There is an added complication with mechanically-driven patterning SPM experiments: above a certain force, the tip begins to wear. In a study on wearing of silicon nitride coatings, one group found that after enough abrasion the nitride coating on an AFM tip begins to delaminate.[102] This effect increases the tip radius of curvature and would be accelerated by elevated applied force required by chemomechanical methods. Tip wear must be evaluated for SPM chemomechanical methods. Both chemomechanical nanografting and related studies on wearing of AFM tips during chemomechanical methods are presented in Chapter 4.[101]

As a method matures, the research moves from theoretical investigation, to process improvement, to practical application. Common applications for nanoscale patterning are electrical circuitry and self-assembly of biological molecules. Chapter 5[103] expands nanografting to include covalent patterning of silicon dioxide, provides the basis for chemomechanical work on silicon dioxide, and presents proof-of-concept applications for mechanically-driven patterning on an insulator. Copper was electrolessly deposited on patterned lines to demonstrate the feasibility of electrical nanocircuitry and DNA was aligned on patterned lines to demonstrate compatibility with biological applications.

The final chapter provides an overview of the work as a whole. An analysis of the aspects relating to portions of work presented in different chapters is described. After this analysis, future work related to chemomechanical functionalization and nanografting is presented. These are encompassed in Chapter 6.

[1] Binnig, G.; Rohrer, H. Scanning apparatus for surface investigation using vacuum-tunnel effect at cryogenic temperatures. US Patent 4,343,993, August 10, 1982.

[2] Eigler, D. M.; Schweizer, E. K. *Nature (London)* **1990**, *344*, 524-6.

[3] Binnig, G.; Quate, C.F.; Gerber, Ch. *Physics Review Letters* **1986**, *56*, 930-933.

[4] Binnig, G.; Gerber, Ch.; Stoll, E.; Albrecht, T. R.; Quate, C. F. *Europhysics Letters* **1987**, *3*, 1281-1286.

[5] Binnig, G.; Gerber, Ch.; Stoll, E.; Albrecht, T. R.; and Quate, C. F. *Surface Science* **1987**, *189/190*, 1-6.

[6] International Technology Roadmap for Semiconductors. http://www.itrs.net/ (Accessed June 25, 2007).

[7] He, H. X.; Li, Q. G.; Zhou, Z. Y.; Zhang, H.; Li, S. F. Y.; Liu, Z. F. *Langmuir*, **2000**, *16*, 9683-9686.

8 Demers, L. M.; Mirkin, C. A. *Angew. Chem. Int. Ed.* **2001**, *40*, 3069-3071.

[9] Fendler, J. H. *Chem. Mater.* **2001**, *13*, 3196-3210.

[10] Buriak, J. M. *Chem. Rev.* **2002**, *102*, 1271-1308.

[11] Cavallini, M.; Mei, P.; Biscarini, F.; Garcia, R. *Applied Physics Letters* **2003**, *83*, 5286-5288.

[12] Kumar, A.; Abbott, N. L.; Kim, E.; Biebuyck, H. A.; Whitesides, G. M. *Acc. Chem. Res.* **1995**, *28*, 219-226.

[13] Mirkin, C. A.; Letsinger, R. L.; Mucic, R. C.; Storhoff, J. J. *Nature* **1996**, *382*, 607-609.

[14] Graber, D. J.; Zieziulewicz, T. J.; Lawrence, D. A.; Shain, W.; Turner, J. N. *Langmuir* **2003**, *19*, 5431-5434.

[15] Pena, D. J.; Raphael, M. P.; Byers, J. M. *Langmuir* **2003**, *19*, 9028-9032.

[16] Hovis, J. S.; Boxer, S. G. *Langmuir* **2001**, *17*, 3400-3405.

[17] Kenseth, J. R.; Harnisch, J. A.; Jones, V. W.; Porter, M. D. *Langmuir* **2001**, *17*, 4105-4112.

[18] Lee, K.-B.; Lim, J.-H.; Mirkin, C. A. *J. Am. Chem. Soc.* **2003**, *125*, 5588-5589.

[19] Cheung, C. L.; Camarero, J. A.; Woods, B. W.; Lin, T.; Johnson, J. E.; De Yoreo, J. J. *J. Am. Chem. Soc.* **2003**, *125*, 6848-6849.

[20] Arkles, B. *Chemtech* **1977**, *7*, 766-778.

[21] Maoz, R.; Sagiv, J.; Degenhardt, D.; Möhwald, H.; Quint, P. *Supramol. Sci.* **1995**, *2*, 9.

[22] Maoz, R.; Matlis, S.; DiMasi, E.; Ocko, B. M.; J. Sagiv *Nature* **1996**, *384*, 150.

[23] Maoz, R.; Sagiv, J. *Adv. Mater.* **1998**, *10*, 580-584.

[24] Maoz, R.; Cohen, S. R.; Sagiv, J. *Adv. Mater.* **1999**, *11*, 55-61.

[25] Maoz, R.; Frydman, E.; Cohen, S. R.; Sagiv, J. *Adv. Mater.* **2000**, *12*, 725-731.

[26] Hoeppener, S.; Maoz, R.; Sagiv, J. *Nano Lett.* **2003**, *3*, 761-767.

[27] Hoeppener, S.; Maoz, R.; Sagiv, J. *Adv. Mater.* **2006**, *18*, 1286–1290.

[28] Maoz, R.; Frydman, E.; Cohen, S. R.; Sagiv, J. *Adv. Mater.* **2000**, *12*, 424- 429.

[29] Liu, S.; Maoz, R.; Schmid, G.; Sagiv, J. *Nano Lett.* **2002**, *2*, 1055-1060.

[30] Wouters, D.; Schubert, U. S. *Langmuir* **2003**, *19*, 9033-9038.

[31] Hoeppener, S.; Maoz, R.; Cohen, S. R.; Chi, L.; Fuchs, H.; Sagiv, J. *Adv. Mater.* **2002**, *14*, 1036-1041.

[32] Robins, E. G.; Stewart, M. P.; Buriak, J. M. *Chem. Commun.* **1999**, 2479–2480.

[33] Hurley, P. T.; Ribbe, A. E.; Buriak, J. M. *J. Am. Chem. Soc.* **2003**, *125*, 11334-11339.

[34] Choi, H. C.; Buriak, J. M. *Chem. Mater.* **2000**, *12*, 2151-2156.

[35] Cai, Y.; Ocko, B. M. *J. Am. Chem. Soc.* **2005**, *127*, 16287-16291.

[36] Jang, S.-Y.; Marquez, M.; Sotzing, G. A. *J. Am. Chem. Soc.* **2004**, *126*, 9476-9477.

[37] Li, Y.; Maynor, B. W.; Liu, J. *J. Am. Chem. Soc*. **2001**, *123*, 2105-2106.

[38] Maynor, B. W.; Li, Y.; Liu, J. *Langmuir* **2001**, *17*, 2575-2578.

[39] Kumar, A.; Whitesides, G. M. *Appl. Phys. Lett.* **1993**, *63*, 2002-2004.

[40] Gates, B. D.; Xu, Q.; Stewart, M.; Ryan, D.; Willson, C. G.; Whitesides, G. M. *Chem. Rev.* **2005**, *105*, 1171-1196.

[41] Xia, Y.; Whitesides, G. M. *Angew. Chem. Int. Ed.* **1998**, *37*, 550-575.

[42] Xia, Y.; Whitesides, G. M. *Annu. Rev. Mater. Sci.* **1998**, *28*, 153–84.

[43] Huck, W. T. S. *Angew. Chem. Int. Ed.* **2007**, *46*, 2754–2757.

[44] Xia, Y.; Tien, J.; Qin, D.; Whitesides, G. M. *Langmuir* **1996**, *12*, 4033-4038.

[45] St. John, P. M.; Craighead, H. G. *Appl. Phys. Lett.* **1996**, *68*, 1022-1024.

[46] Kim, E.; Kumar, A.; Whitesides, G. M. *J. Electrochem. Soc.* **1995**, *142*, 628-633.

[47] Whidden, T. K.; Ferry, D. K.; Kozicki, M. N.; Kim, E.; Kumar, A.; Wilbur, J.; Whitesides, G. M. *Nanotechnology* **1996**, *7*, 447–451.

[48] Xia, Y.; Mrksich, M.; Kim, E.; Whitesides, G. M. *J. Am. Chem. Soc.* **1995**, *117*, 9576-9577.

[49] Jeon, N. L.; Nuzzo, R. G.; Xia, Y.; Mrksich, M.; Whitesides, G. M. *Langmuir* **1995**, *21*, 3024-3026.

[50] Bernard, A.; Delamarche, E.; Schmid, H.; Michel, B.; Bosshard, H. R.; Biebuyck, H. *Langmuir*, **1998**, *14*, 2225-2229.

[51] Hidber, P. C.; Helbig, W.; Kim, E.; Whitesides, G. M. *Langmuir* **1996**, *12*, 1375-1380.

[52] Gates, B. D.; Xu, Q.; Love, J. C.; Wolfe, D. B.; Whitesides, G. M. *Annu. Rev. Mater. Res.* **2004**, *34*, 339–372.

[53] Piner, R. D.; Zhu, J.; Xu, F.; Hong, S.; Mirkin, C. A. *Science* **1999**, *283*, 661-663.

[54] Ivanisevic, A.; Mirkin, C. A. *J. Am. Chem. Soc*. **2001**, *123*, 7887-7889.

[55] Wang, Y.; Zhang, Y.; Li, B.; Lü, J.; Hub, J. *Appl. Phys. Lett.* **2007**, *90*, 133102.

[56] Hong, S.; Zhu, J.; Mirkin, C. A. *Science* **1999**, *286*, 523-525.

[57] Weinberger, D. A.; Hong, S.; Mirkin, C. A.; Wessels, B. W.; Higgins, T. B. *Adv. Mater.* **2000**, *12*, 1600-1603.

[58] Demers, L. M.; Park, S.-J.; Taton, T. A.; Li, Z.; Mirkin, C. A. *Angew. Chem. Int. Ed.* **2001**, *40*, 3071-3073.

[59] Zou, S.; Maspoch, D.; Wang, Y.; Mirkin, C. A.; Schatz, G. C. *Nano Letters* **2007**, *7*, 276-280.

[60] Jang, J.; Hong, S.; Schatz, G. C.; Ratner, M. A. *J. Chem. Phys.* **2001**, *115*, 2721-2729.

[61] Hong, S.; Zhu, J.; Mirkin, C. A. *Langmuir* **1999**, *15*, 7897-7900.

[62] Jang, J.-W.; Maspoch, D.; Fujigaya, T.; Mirkin, C. A. *Small* **2007**, *3*, 600 – 605.

[63] Abbott, N. L.; Folkers, J. P.; Whitesides, G. M. *Science* **1992**, *257*, 1380-1384.

[64] Xu, S.; Liu, G.-y. *Langmuir* **1997**, *13*, 127-129.

[65] Xu, S.; Laibinis, P. E.; Liu, G.-y. *J. Am. Chem. Soc.* **1998**, *120*, 9356-9361.

[66] Liu, M.; Liu, G.-y. *Langmuir* **2005**, *21*, 1972-1978.

[67] Jiang, G.; Niederhauser, T. L.; Fleming, S. A.; Asplund, M. C.; Linford, M. R. *Langmuir* **2004**, *20*, 1772-1774.

[68] Niederhauser, T. L.; Jiang, G.;Lua, Y.-Y.; Dorff, M. J.; Woolley, A. T.; Asplund, M. C.; Berges, D. A.; Linford, M. R. *Langmuir* **2001**, *17*, 5889-5900.

[69] Yang, L.; Lua, Y.-Y.; Lee, M. V.; Linford, M. R. *Acc. Chem. Res.* **2005**, *38*, 933-942.

[70] Wacaser, B. A.; Maughan, M. J.; Mowat, I. A.; Niederhauser, T. L.; Linford, M. R.; Davis, R. C. *Appl. Phys. Lett.* **2003**, *82*, 808-810.

[71] Moore, S. K. "Just One Word-Plastics" Special R and D Report *IEEE Spectrum Online* http://www.spectrum.ieee.org/print/1638 (accessed July 17, 2007).

[72] "Alternative Storage/ Patterned Magnetic Media" Hitachi research article. http://www.hitachigst.com/hdd/research/storage/alternative_storage/pm.html (accessed July 17, 2007).

[73] Linford, M. R. "Producing coated particles by grinding in the presence of reactive species" US Patent 6,132,801, October 17, 2000.

[74] Niederhauser, T. L.; Lua, Y.-Y.; Jiang, G.; Davis, S. D.; Matheson, R.; Hess, D. A.; Mowat, I. A.; Linford, M. R. *Angew. Chem., Int. Ed. Engl.* **2002** *13*, 2353.

[75] Lua,Y.-Y.; Fillmore, W. J. J.; Linford, M. R. Appl. Surf. Sci. **2004**, *231-232*, 323.

[76] Niederhauser, T. L.; Lua, Y.-Y.; Sun, Y.; Jiang, G.; Strossman, G. S.; Pianetta, P.; Linford, M. R. *Chemistry of Materials* **2002**, *14*, 27.

[77] Lua, Y.-Y.; Lee, M. V.; Fillmore, W. J. J.; Matheson, R.; Sathyapalan, A.; Asplund, M. C.; Fleming, S. A.; Linford, M. R. *Angew. Chem., Int. Ed. Engl.* **2003**, *42*, 4046.

[78] Lua,Y.-Y.; Fillmore, W. J. J.; Yang, L.; Lee, M. V.; Savage, P. B.; Asplund, M. C.; and Linford, M. R. *Langmuir* **2005**, *21*, 2093.

[79] Wolkow, R. A. *Annu. Rev. Phys. Chem.* **1999**. *50*, 413–441.

[80] Linford, M. R.; Chidsey, C. E. D. *J. Am. Chem. Soc.* **1993**,*115*, 12631-12632.

[81] Linford, M. R.; Fenter, P.; Eisenberger, P. M.; Chidsey, C. E. D. *J. Am. Chem. Soc.* **1995**, *117*, 3145-3155.

[82] Cicero, R. L.; Linford, M. R.; Chidsey, C. E. D. *Langmuir* **2000**, *16*, 5688-5695.

[83] Jiang, G.; Niederhauser, T. L.; Davis, S. D.; Lua, Y.-Y.; Cannon, B. R.; Dorff, M. J.; Howell, L. L.; Magleby, S. P.; Linford, M. R. *Colloids and Surfaces A: Physicochemical and Engineering Aspects* **2003**, *226*, 9.

[84] Barriocanal, J. A.; Doren, D. J. *J. Am. Chem. Soc.* **2001**, *123*, 7340-7346.

[85] Hess, J. S.; Doren, D. J. *J. Phys. Chem. B* **2002**, *106*, 8206-8210.

[86] Mulcahy, C. P. A.; Carman, A. J.; Casey, S. M. *Surface Science* **2000**, *459*, 1-13.

[87] Wang, G. T.; Mui, C.; Musgrave, C. B.; Bent, S. F. *J. Phys. Chem. B* **1999**, *103*, 6803-6808.

[88] Hamers, R. J.; Hovis, J. S.; Greenlief, C. M.; Padowitz, D. F. *Jap. J. App. Phys.* **1999**, *38*, 3879-3887.

[89] Hamers, R. J.; Hovis, J. S.; Lee, S.; Liu, H.; Shan, J. *Physical Chemistry B* **1997**, *101*, 1489-1492.

[90] Mui, C.; Bent, S. F.; Musgrave, C. B. *J.Phys.Chem.A* **2000**, *104*, 2457-2462.

[91] Kim, W.; Kim, H.-N.; Lee, G. U.; Hong, Y.-K.; Lee, K.; Hwang, C.; Kim, D.-H.; Koo, J.-Y. *Phys. Rev. B* **2001**, *64*, 193313.

[92] Morikawa, Y. *Phys. Rev. B* **2001**, *63*, 033405.

[93] Lu, X. *J.Am.Chem.Soc.* **2003**, *125*, 6384-6385.

[94] Sieval, A. B.; van den Hout, B.; Zuilhof, H.; Sudholter, E. J. R. *Langmuir* **2000**, *16*, 2987-2990.

[95] Sieval, A. B.; van den Hout, B.; Zuilhof, H.; Sudholter, E. J. R. *Langmuir* **2001**, *17*, 2172-2181.

[96] Lee, M. V.; Guo, D.; Linford, M. R.; Zuilhof, H. *Langmuir* **2004**, *20*, 9108-9113.

[97] Lua, Y.-Y.; Niederhauser, T. L.; Wacaser, B. A.; Mowat, I. A.; Woolley, A. T.; Davis, R. C.; Fishman, H. A.; Linford, M. R. *Langmuir* **2003**, *19*, 985-988.

[98] Cannon, B. R.; Magleby, S. P.; Howell, L. L.; Jiang, G.; Niederhauser, T. L.; Linford, M. R. *Proceedings of the 2002 ASME International Mechanical Engineering Congress and Exposition* November 17-22, **2002**, New Orleans, LA. IMECE2002/33554

[99] Lee, M. V.; Richards, J. L.; Linford, M. R.; Casey, S. M. *J. Vac. Sci. Technol. B* **2006**, *24*, 750-755.

[100] Helt, J. M.; Batteas, J. D. *Langmuir* **2006**, *22*, 6130-6141.

[101] Lee, M. V.; Hoffman, M. T.; Barnett, K.; Geiss, J.-M.; Smentkowski, V. S.; Linford, M. R.; Davis, R. C. *Journal of Nanoscience and Nanotechnology* **2006**, *6*, 1639-1643.

[102] Wang, D. F.; Kato K. *Journal of Tribology* **2003**, *125*, 430-436.

[103] Lee, M. V.; Nelson, K. A.; Hutchins, L.; Becerril, H. A.; Cosby, S. T.; Blood, J. C.; Wheeler, D. R.; Davis, R. C.; Woolley, A. T.; Harb, J. N.; Linford, M. R. *Submitted to Chemistry of Materials*.

Chapter 2. Molecular modeling of alkyl monolayers on the Si(100)-2x1 surface*

Michael V. Lee,[†] Dawei Guo,[‡] Matthew R. Linford,[†] and Han Zuilhof[‡]

Abstract

Molecular modeling was used to simulate various surfaces derived from the addition of 1-alkenes and 1-alkynes to Si=Si dimers on the Si(100)-2x1 surface. The primary aim was to better understand the interactions between adsorbates on the surface and distortions of the underlying silicon crystal due to functionalization. Random addition of ethylene and acetylene was used to determine how the addition of an adduct molecule affects subsequent additions for coverages up to one molecule per silicon dimer, *i.e.*, 100% coverage. Randomization subdues the effect that the relative positions of the adsorbates have on the enthalpy of the system. For ethylene and acetylene the enthalpy of reaction changes less than 3 kcal/mol and 5 kcal/mol, respectively, from the first reacted species up to 100% coverage. As a result, a (near-) complete coverage is predicted, which is in line with experimental data. When 1-alkenes and 1-alkynes add by [2+2] addition, the hydrocarbon chains interact differently depending on the direction they project from the surface. These effects were investigated for 4-carbon chains: 1-butene and 1-butyne. As expected, the chains that would otherwise intersect bend to avoid each other; raising

---

* Reproduced with permission from Michael V. Lee, Dawei Guo, Matthew R. Linford, and Han Zuilhof "Molecular Modeling of Alkyl Monolayers on the Si(100)-2 x 1 Surface" *Langmuir* **2004**, *20*, 9108-9113. [doi: 10.1021/la048894e]

[†] Department of Chemistry and Biochemistry, Brigham Young University, Provo, UT 84602 USA

[‡] Laboratory of Organic Chemistry, Wageningen University, Dreijenplein 8, 6703 HB Wageningen, The Netherlands

the enthalpy of the system. For alkyl chains longer than 4-carbons, the chains are able to reorient themselves in a favorable manner, thus resulting in a steady reduction in reaction enthalpy of about 2 kcal/mol for each additional methylene unit.

Overview

Due to silicon's central role in modern semiconducting manufacturing and micromachining, there has recently been significant interest in functionalizing its surface with organic monolayers.[1,2,3,4,5,6,7] The silicon surface may appear as a reconstruction, *e.g.*, Si(100)-2x1 or Si(111)-7x7,[8,9,10,11,12,13] as planar (Si(111)-H or Si(100)-H_2)[14,15,16,17,18,19,20] or porous hydrogen-terminated silicon,[21,22,23,24] or as ground[25,26] or scribed silicon.[26,27,28,29,30] Some of the most important chemistry for all of these surfaces is their reaction with carbon-carbon double or triple bonds. In particular, 1-alkenes and 1-alkynes undergo a [2+2] addition onto the silicon-silicon dimer of Si(100)-2x1 to form four-membered rings that contain two carbon-silicon single bonds in a "di-σ" configuration. This di-σ configuration is the most likely mode of binding and is used in this work.[31] Other bonding configurations for acetylene, including "end-bridge" and "tetra-σ," have also been proposed.[31,32,33,34] Ethylene and acetylene react with the Si(100) reconstructed surface at 100% coverage, but after 50% coverage high dosages are required to functionalize the remaining surface.[9,35,36,37]

Alkyl chains in monolayers on silicon derived from 1-alkenes and 1-alkynes are tethered through robust carbon-silicon bonds, and have been characterized by many techniques including X-ray photoelectron spectroscopy, infrared spectroscopy, optical ellipsometry, wetting, Auger electron spectroscopy, X-ray reflectivity, atomic force microscopy, time-of-flight secondary ion mass spectrometry, and scanning tunneling

microscopy.[2,4,38] Molecular modeling is another important tool for studying monolayers on silicon because it can help confirm and even predict the conformation and binding of individual alkyl chains in an ensemble of alkyl chains. Thus, molecular modeling complements the large number of experimental techniques that provide average properties of alkyl chains in monolayers, but with which the specific, microscopic picture afforded by molecular modeling is difficult to obtain. Indeed, molecular modeling also allows one to create "materials" and to perform "experiments" that would be difficult or impossible to make or perform in a laboratory. For example, Sudhölter, Zuilhof, and coworkers modeled different substitution percentages of 1-octadecene on Si(111)-H.[39,40] They showed that ~50% surface substitution was most favorable, in good agreement with experimental results. This work demonstrated the importance of using large enough dimensions of a repeat unit in simulations with periodic boundary conditions, as well as the power of boundary conditions to reduce computational requirements while simultaneously improving the accuracy of results. Ma and coworkers also used molecular simulation models and quantum chemistry to study the formation mechanisms and packing structures of alkoxyl and alkyl monolayers on hydrogen-terminated Si(111).[41] Tao and coworkers similarly modeled self-assembled monolayers on gold and found that the packing of alkyl chains and aromatic groups was the primary factor in determining substitution coverage.[42]

Here we present a molecular modeling study of monolayers of 1-alkenes and 1-alkynes on Si(100)-2x1, which is silicon's most studied and important reconstruction.[2,4] While a number of *ab initio* calculations of the reaction of one or even a few reactive molecules with Si(100)-2x1 have been performed,[9,32,34,36] we are not aware of any molecular

modeling study of alkyl monolayers on reconstructed Si(100). Here we find that molecular modeling studies support the 100% coverages found experimentally for ethylene (see Figure 1) and acetylene, and may provide some insight into the reasons for the reduced sticking coefficient after 50% coverage. The results also indicate that 100% coverage becomes more favored for longer 1-alkene and 1-alkyne hydrocarbons without regard to their orientation on the surface. An additional motivation for this study is that Si(100)-2x1 is believed to be a good model surface for chemomechanically scribed silicon.[26,27,28,29,30]

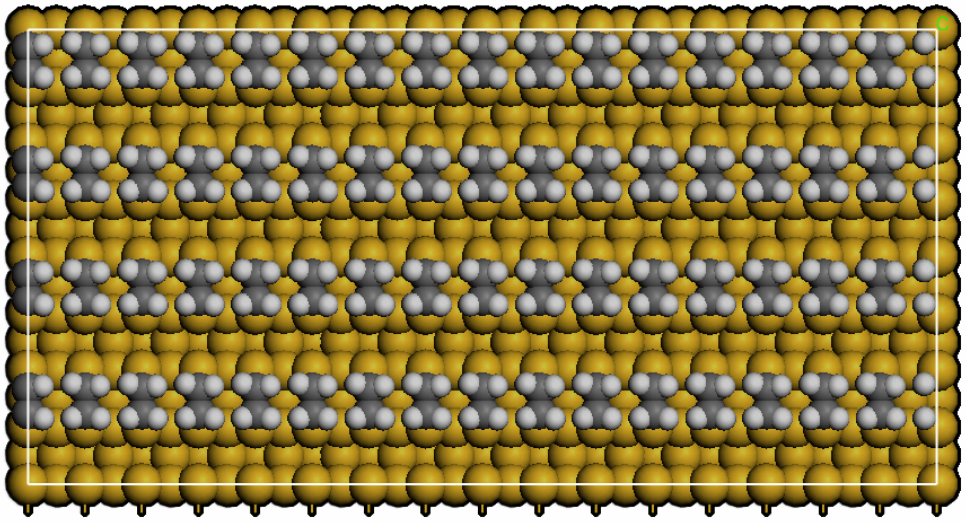

Figure 1. Top view of four dimer rows, each containing sixteen dimers, of Si(100)-2x1 saturated with ethylene. Yellow is silicon, gray is carbon, white is hydrogen.

Experimental

General methodological details

All simulations were performed with the Accelrys Materials Studio PC software package using its implementation of the COMPASS[43,44] force field. For the simulations, a Si(100) model surface was created by cleaving a silicon crystal structure at the <100> plane. The basic Si(100) cell that was used was 3.840 Å x 7.680 Å on the 100 surface and

includes one complete bulk silicon unit cell below the reconstructed surface. Hydrogen atoms were added to the bottom of the silicon unit cell to avoid dangling bonds. The bottom layer of silicon atoms was fixed in each simulation to occupy silicon lattice positions. The positions of the hydrogen atoms on the bottom of the lattice were also fixed in all iterations of all simulations. Each simulated structure was created on this basic Si(100) reconstructed surface cell. The resulting surfaces were optimized with the Materials Studio "Fine" convergence settings with atom-based summation for "vdW and Coulomb" non-bond calculations. Application of repeating boundary conditions in Materials Studio treats the structure as if it were repeated in three and not just two dimensions.[39,40] Therefore, a 20 Å vacuum slab was added and the "long-range correction" was deactivated to avoid interaction between successive cells in the vertical direction, *i.e.*, these corrections eliminated interactions between the atoms at the top of the monolayer lattice and the hydrogen atoms at the bottom of the "next" silicon lattice. [39,40] In the case of the extended chain simulations, the initial vacuum slab was 100 Å to allow ample room for longer chains. Although periodic boundary conditions were applied to simulate a larger surface, no symmetry constraints were applied to the repeated surface.

To compare different simulations the average enthalpy of the reaction per chain (E_{rxn}) was calculated from the minimized enthalpies (E_{min}), which are the output from Materials Studio. The average enthalpy change per chain (E_{rxn}) equals the minimized enthalpy (E_{min}) less the bare surface enthalpy and enthalpy for the free adsorbate, divided by the number of substituted dimers.

Random coverage simulations

The surfaces for the random coverage simulations were made by first creating an array of four dimer rows, each containing sixteen dimers, where each dimer was saturated with ethylene (see Figure 1) or acetylene. A certain number of ethylene or acetylene molecules was then randomly removed. To accomplish this each position was assigned a number. Using random numbers that were mostly generated from atmospheric noise (***e.g.***, www.random.org) it was determined which positions should remain substituted, ***e.g.***, for 25% coverage sixteen different random numbers from 1 to 64 were produced to designate the positions that should remain covered. The carbon and hydrogen atoms were then removed from the dimers that were not designated, and their respective Si=Si dimers were reformed. In this manner all desired degrees of coverage and substitution patterns could be obtained. Random coverages between 0 and 100% were produced.

For acetylene substitution this straightforward procedure worked seamlessly, but for ethylene substitution the full optimization failed in all but two cases (12.5% and 100% coverage). In the cases where full geometry optimization failed, global optimization could only be approximated in a stepwise fashion. We chose to use an iterative process whereby the coordinates of either the ethylene moieties or the silicon atoms were fixed while the other set of atoms was optimized. In the next step the atoms that had been optimized were fixed, and those that had been fixed were released and optimized. This process was continued until the difference between subsequent optimizations of the ethylene moieties was less than 0.02 kcal/mol per substituted site and always less than 1 kcal/mol in total. Because Materials Studio accounts for fixed or non-fixed atoms differently, the minimal energy that was finally obtained (E_{min} for the iterative

optimization) was calculated by releasing all atoms and performing a single-point energy calculation.

This iterative procedure could be compared to the standard full optimization for both 12.5% (8/64 substitutions) and 100% (64/64 substitutions) coverages. The results of the iterative optimization and the full optimization differed by less than 0.5 kcal/mol for 100% coverage (*i.e.*, less than 0.01 kcal/mol per chain) and less than 0.2 kcal/mol for the 12.5% coverage (*i.e.*, less than 0.03 kcal/mol per chain). The similarity on the resulting optimized energies shows the consistency of this iterative approach with the automated optimization.

Surface patterns

The 1-butene and 1-butyne surface patterns were created from a single dimer cell of ethylene or acetylene, respectively. This unit cell was doubled in both directions to form a cell of four dimers. One of the hydrogen atoms in each of the substituted dimers was then replaced with an ethyl ($-CH_2CH_3$) group to form a series of desired patterns. These unit cells of four dimers were then expanded to create a surface of four dimer rows with eight dimers to a row. E_{rxn} was then calculated for each pattern.

Extended chains

In order to explore the effect that longer 1-alkenes and 1-alkynes have on the surface, the chains from the surface patterns that were derived from four-carbon adsorbates were extended, and the energy of the resulting surface was minimized. In this procedure, a hydrogen atom at the end of the tethered chain was replaced with a methyl ($-CH_3$) group, and the surface was then re-minimized. This methyl group was typically added to

continue the mostly-trans configuration of the chain. The chains were incrementally extended in this fashion until they were sixteen carbons long.

Results and discussion

Model verification

Prior to viewing the results predicted by a model, it is important for it to be validated. In this section it is confirmed that the bond distances predicted by the simulation are reasonable, and that a sufficiently large silicon lattice is chosen. A comment on the effectiveness of the COMPASS force field is then made.

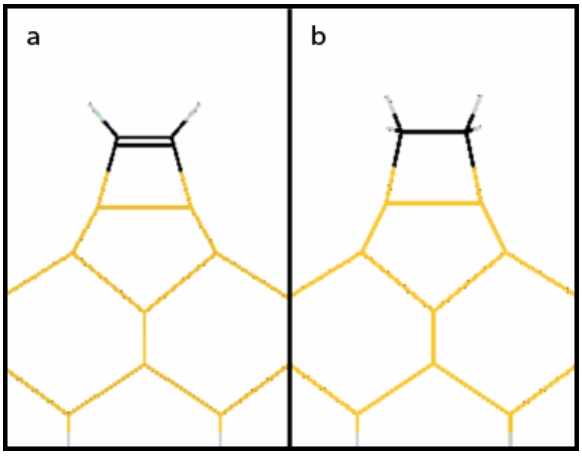

Figure 2. Minimized structures for (a) acetylene and (b) ethylene on the Si(100) dimer. C=C, Si-C, Si-Si bond lengths for 100% acetylene are 1.357 Å, 1.835 Å, 2.357 Å; for a single acetylene the bond lengths are 1.357 Å, 1.841 Å, 2.265 Å. C-C, Si-C, Si-Si bond lengths for 100% ethylene are 1.629 Å, 1.916 Å, 2.381 Å; for a single ethylene they are 1.628 Å, 1.922 Å, and 2.356 Å. Yellow represents silicon, black represents carbon, and gray represents hydrogen.

The C-C, C=C, Si-C, and Si-Si bond lengths for the four-membered ring for chemisorbed ethylene and acetylene on Si(100)-2x1 have been determined in a number of theoretical and experimental studies.[31,38,39,40] For ethylene adsorption the Si-Si and Si-C bond lengths range from 2.33 to 2.37 Å or 1.90 to 1.96 Å, respectively, and for acetylene they range from 2.23 to 2.44 Å or 1.83 to 1.98 Å, respectively. These values compare

favorably with those reported in this work. As expected, the bond lengths vary slightly depending on the degree of coverage (see Figure 2).

In order to determine the repeat unit size for the calculations, a single adsorbate molecule was placed on a surface and the structure was minimized (both ethylene and acetylene were considered). Starting at the point of substitution, the distances between successive dimers along the dimer row (moving perpendicular to the C-C or C=C bond in the adsorbed species) were measured. It was found that the distance between dimers more than four dimers away from the substituted site were within 1% of the distance between dimers in unsubstituted Si(100)-2x1. Similarly, the length of the neighboring Si=Si dimer on the adjacent dimer row from the substituted site (moving parallel to the C-C or C=C bond in the adsorbed species) was within 0.05% of the Si=Si dimer length for bare silicon. A repeat unit of four rows with eight dimers each was chosen for the surface patterns of the four-carbon adsorbates (vide infra), which was extended for the random coverage simulations to four rows with sixteen dimers each to create more sites.

No proper parameterization of the Si=Si dimer is present in the standard COMPASS force field. However, we were only interested in accurate trends and not absolute energies. Therefore, because the constant error in the absolute energies has no impact on the relative energies presented here, the error in absolute addition enthalpies was left uncorrected in this work.

Complete and random coverages of two-carbon adsorbates

The simulations of 100% substitution of both ethylene and acetylene present interesting results relevant to the entire project. Figure 3 and Figure 4 show the minimized surfaces for ethylene and acetylene, respectively. It is apparent from Figure 3 that steric

interactions between chemisorbed ethylene molecules are large and cause a distortion of the surface yielding a structure with pm symmetry, in which the four-membered rings are not perpendicular to the surface. In contrast, chemisorbed acetylene molecules on adjacent dimer rows are exactly in line with each other (Figure 4), yielding a surface with ppm symmetry, which points to only a limited inter-adduct interaction.

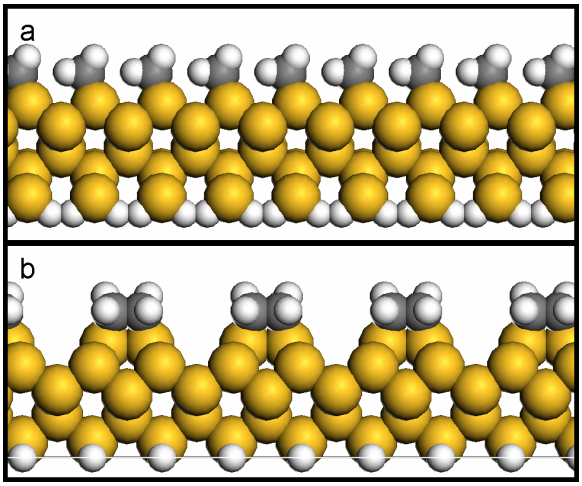

Figure 3. Ethylene on Si(100)-2x1 at 100% coverage. a) View perpendicular to the carbon-carbon bond. b) View parallel to the carbon-carbon bond. The yellow, black, and gray atoms are from silicon, carbon and hydrogen, respectively. Hydrogens on adjacent molecules in (a) are 5.316 Å and 5.339 Å apart for the elevated and depressed hydrogens, respectively. Nearest hydrogens between molecules in (b) are 2.424 Å apart.

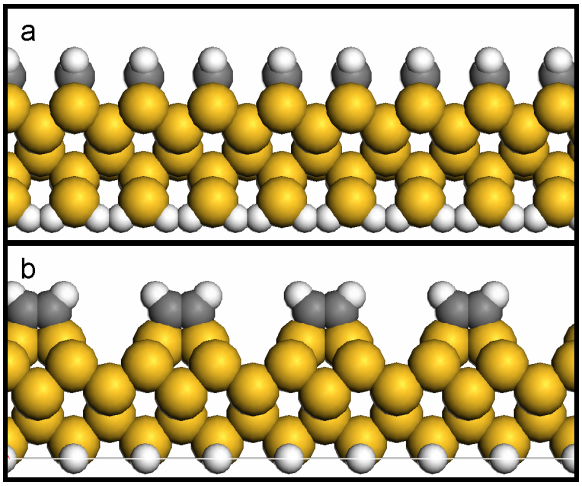

Figure 4. Acetylene on Si(100)-2x1 at 100% coverage. a) View perpendicular to the carbon-carbon double bond. b) View parallel to the carbon-carbon double bond. The yellow, black, and gray atoms are from silicon, carbon and hydrogen, respectively. Distances between hydrogens on adjacent molecules are 4.908 Å and 3.840 Å apart for (a) and (b), respectively.

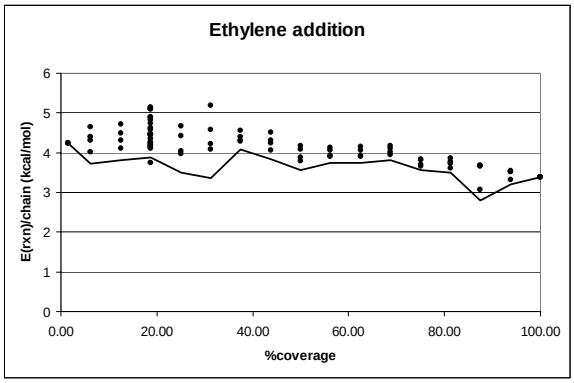

Figure 5. E_{rxn} values for ethylene adsorption on Si(100)-2x1 for coverages ranging from 0 to 100%. Based on the variation in the data, 95% of the randomized results for a given coverage should lie above the line. Four simulations were performed at each coverage, except at 18.75% coverage where 21 simulations were performed.

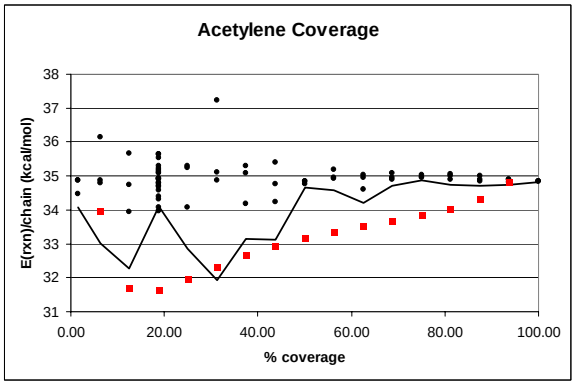

Figure 6. E_{rxn} values for acetylene adsorption on Si(100)-2x1 for coverages ranging from 0 to 100%. Three simulations were performed at each coverage, except at 18.75% coverage where 21 simulations were performed. Based on the variation in the data, 95% of the randomized results for a given coverage should lie above the line. Red squares indicate E_{rxn} for grouped acetylene molecules.

As shown in Figure 5 and Figure 6 the energy per addition to the Si(100)-2x1 surface for both ethylene and acetylene does not change significantly upon addition of more chains to the surface. The enthalpy per ethylene chain decreases from *ca.* 4.5 kcal/mol to 3.5 kcal/mol. The enthalpy per acetylene chain added in a randomized pattern stays close to 35 kcal/mol. Figure 5 and Figure 6 include lines that define the 95% confidence interval for a t distribution for each set of simulations, *i.e.*, for a normal distribution 95% of the values for E_{rxn} for a certain coverage should lie above this line. Thus, this line approximates the minimum enthalpy per chain, E_{rxn}, for each random coverage. Given the

possibility for a direct comparison with experimental data, it is most clarifying to start with the acetylene addition. We note that the minimum energy required for addition of each acetylene molecule is 32-33 kcal/mol for 0 – 50% coverage, and 34-35 kcal/mol for 50-100% coverage (Figure 6). This increase in enthalpy between 50 and 100% coverage agrees with results from other calculations,[33,36,37] and the difference of about 2 kcal/mol corresponds well to the 0.19 eV difference between 50 and 100% coverage found by Miotto *et al.* [36] The energy required for an ethylene molecule to react with the Si(100) surface appears to remain relatively constant or to drop somewhat from the first addition up to 100% coverage. The near constant or slightly decreasing values for ethylene in Figure 5 and the results for acetylene adsorption in Figure 6 indicate that attractive Van der Waals interactions between chains at adjacent sites play a more dominant role for ethylene addition than for acetylene addition for coverages higher than 50%.

The twenty-one simulations performed at 18.75% coverage (see Figure 5 and Figure 6) provided us with the opportunity to search for adsorption patterns that might lead to lower surface energy. It was noted for ethylene and acetylene adsorption that the energy of the system seemed to be lower when the adsorbates were adjacent to each other. This hypothesis was tested with acetylene (see Figure 6). A surface was created with four adjacent acetylene molecules, one on each dimer row, *i.e.*, all of the C=C bonds ran along the same straight line, after which acetylene molecules were added sequentially in increments of four in a line next to the previous line. These patterns of grouped acetylene adducts gave the lowest observed enthalpies, the value of which correlates quite well with the 95% confidence interval line in Figure 6. In addition, the reaction enthalpy per chain of such well-controlled grouped attachment increases monotonically, which is in line

with experimental data (vide supra). From such detailed comparisons it becomes clear that there is a delicate balance between energy-raising steric repulsions that lead to, for example, Si-Si-C bond angle bending, and energy-lowering attractive forces. Apparently these counter-acting effects are energetically optimized in patterns of large groups of otherwise empty surfaces. Testing such a hypothesis would be very difficult experimentally. Thus these results demonstrate the importance of molecular modeling and other simulations in materials chemistry.

Surface patterns of four-carbon adsorbates.

The main steric interactions between side chains on adjacent substituted 1-alkenes and 1-alkynes on the Si(100) surface are most clearly illustrated by the interactions between adsorbates with only a few carbon atoms, since longer chains have more rotational degrees of freedom to orient themselves into their lowest energy configurations. To study these interactions, a series of unit cells containing four-carbon adsorbates were created to represent the steric interactions of a side chain with different orientations, as shown in Figure 7 and Figure 8 for [2+2] addition of 1-butene and 1-butyne, respectively. In this manner the primary short-chain effects were explored. For 1-butene addition onto a surface, 4 spatially different orientations of the ethyl group can be distinguished (labeled A to D); for 1-butyne attachment only 2 such positions can be distinguished (labeled E and F).

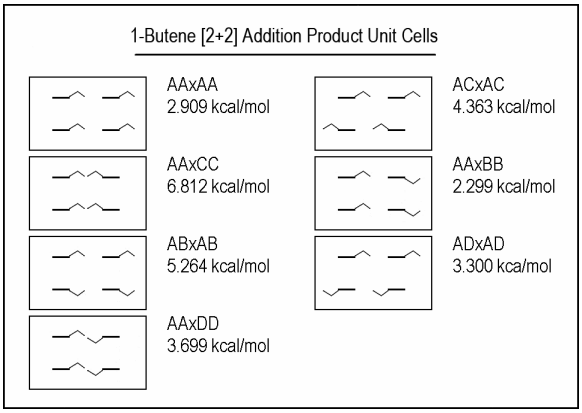

Figure 7. Basic unit cells for pattern investigation of 1-butene [2+2] addition to a reconstructed Si(100) surface. The bold horizontal line represents carbons from the double bond in the original butene molecule. Thinner lines represent carbon chains extending from the surface. Hydrogen atoms are not shown. Values are E_{rxn} for each pattern.

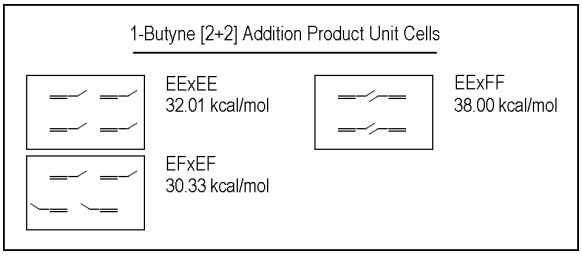

Figure 8. Three unit cells for pattern investigation of 1-butyne [2+2] addition to the reconstructed Si(100) surface. The horizontal double line represents the carbon-carbon double bond above a silicon dimer. Thinner lines represent the carbon chain extending away from the double bond. Hydrogen atoms are not shown. Values are E_{rxn} for each pattern.

The E_{ave} values for these different orientations are given in Figure 7 and Figure 8. The least favorable orientations occur when chains point toward each other. These configurations cause distortions in the silicon lattice, as illustrated in Figure 9, and contribute to the increased energy for the 1-butyne pattern "EE x FF" and for the 1-butene patterns "AA x CC", and "AA x DD". The "AB x AB" pattern for 1-butene also has high energy because the third and fourth carbons of adjacent adsorbates (in the figure lying under or above each other) extend into the same space along a dimer row.

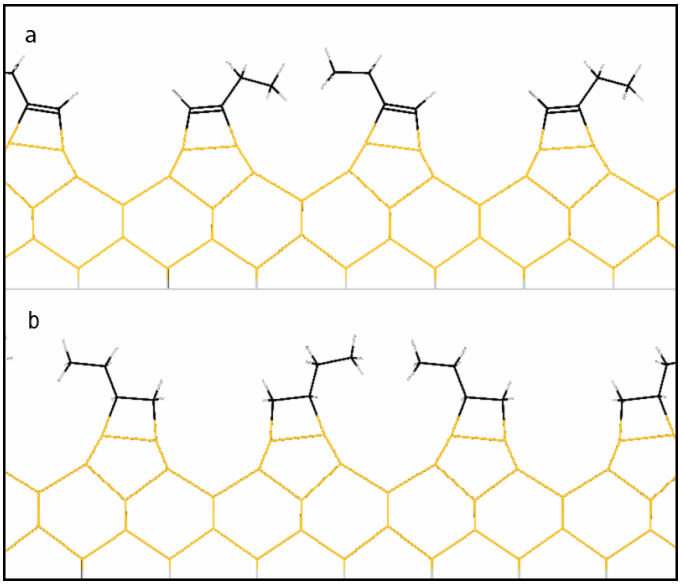

Figure 9. (a) The 1-butyne addition pattern "EE x FF". (b) The 1-butene addition pattern "AA x CC". The views shown are perpendicular to the C-C and C=C bonds, respectively. The adjacent dimers push away from each other and distort the silicon lattice. Silicon atoms are yellow, carbon atoms are black, and hydrogen atoms are gray.

Extended chains

Once the short chain interactions were determined, the chains could be extended to demonstrate the decrease in energy due to favorable van der Waals interactions between longer chains. As the chains reach further from the surface, they have increasing rotational freedom to reorient themselves to low energy configurations. A typical reorientation is shown in Figure 10. Because there is ample room for the chains away from the surface, each additional carbon lowers the energy per substituted chain. This was demonstrated by extending the length of the chains for the lowest enthalpy 1-butene patterns: AAxAA, AAxBB, and ADxAD and the lowest enthalpy 1-butyne patterns: EExEE and EFxEF. That is, the four carbon chains shown in Figure 7 and Figure 8 were extended incrementally to 16 carbon chains. The energy per chain for each chain length is plotted in Figure 11 and Figure 12. These results show a general monotonic decrease as the chains are lengthened. With ever increasing lengths, the size of the stabilization

provided by the inter-chain Van der Waals forces becomes even larger than the stabilization or destabilization provided by the orientation of the adduct on the surface (note n = 5 in Figure 11 and especially Figure 12 where the chains are long enough to interact with the molecule on the next dimer, but not long enough to have additional orientation constraints).

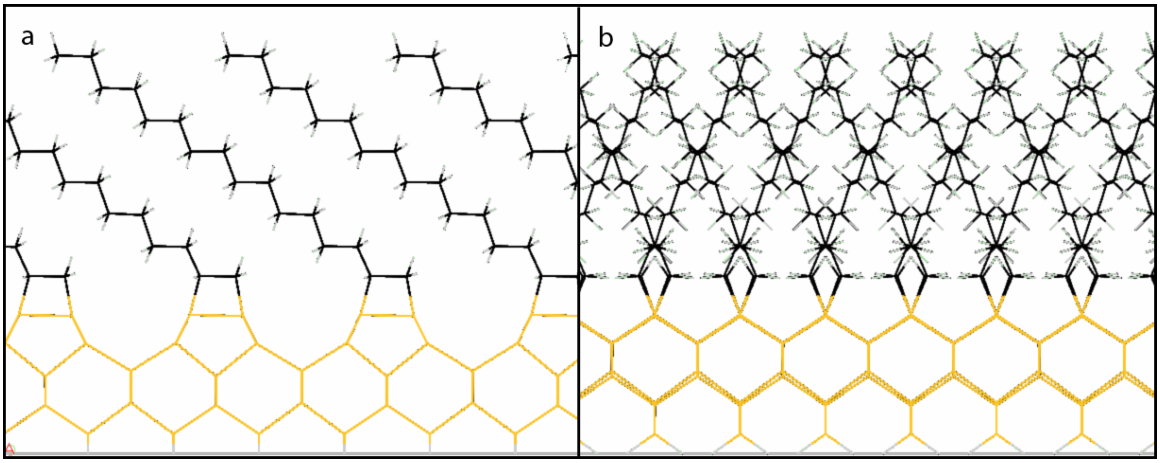

Figure 10. 100% coverage of 1-hexadecene on Si(100)-2x1. (a) View perpendicular to carbon-carbon bond. (b) View along the C-C bond. Although it appears in (a) that the hydrogen atoms point at the hydrogen atoms on the adjacent chain, from (b), one observes that the chains from each dimer row slant in two different, alternating directions and that the hydrogen atoms on one chain interlace with hydrogen atoms on adjacent hydrocarbon chains. Silicon is represented in yellow, carbon in black, and hydrogen in gray. The hydrogens extending from the four-member ring in the direction opposite the chain come the closest to the neighboring chain at 2.057 Å. Further from the surface, the distance between neighboring hydrogens in (a) range from 2 to 5 Å because of the mismatch shown in (b). The distance between hydrogens on parallel chains in (b) range from 2.20 to 2.28 Å.

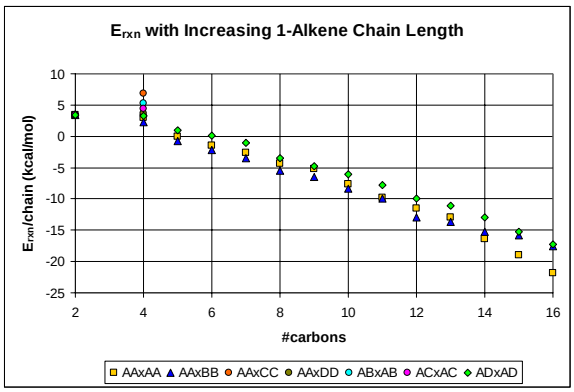

Figure 11. E_{rxn} for addition of 2 to 16 carbon 1-alkenes to Si(100)-2x1 at 1 monolayer coverage for three different attachment patterns (AA x AA, AA x BB and AD x AD, see text).

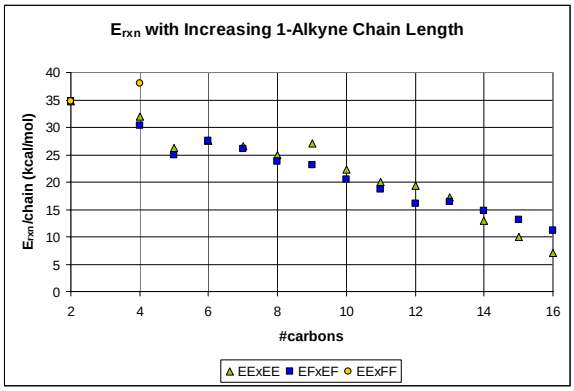

Figure 12. E_{rxn} for addition of 2 to 16 carbon 1-alkynes to Si(100)-2x1 at 1 monolayer coverage for two different attachment patterns (EE x EE and EE x FF, see text).

Conclusion

Molecular mechanics simulations for the addition of ethylene and acetylene onto the reconstructed Si(100)-2x1 surface indicate a near-constant enthalpy for coverages from 0 to 100%. As a result, near-complete surface coverages are likely. Assuming the hydrocarbons can approach the surface, 100% coverage should also be favored for attachment of longer 1-alkenes and 1-alkynes.

Acknowledgment

MRL thanks the Petroleum Research Fund, the Research Corporation, Brigham Young University, and Drs. Howell and Magleby (BYU Mechanical Engineering) for support for this research. HZ thanks Wageningen University and graduate school VLAG for financial support.

Attribution

Dr. Zuilhof and I designed the set of experiments and the method for comparing different experiments with different substituents and different coverages. Dr. Zuilhof also provided critical experience modeling monolayers on silicon. Dawai Guo trained me on

the use of the Materials Studio program. I created all of the simulations used in this work, which includes choosing the surface patterns that represent possible interactions, randomizing the coverages, and creating the modeled surfaces with substituent attached to silicon. I ran all of the simulations except a few that had to be repeated after I returned to the United States. In which case, the files were sent to Dawai Guo, who ran the simulations and returned the output files for interpretation. Dr. Linford provided critical understanding of the scribed silicon surface and its reactivity and also initiated the endeavor.

---

[1] Sieval, A. B.; Linke, R.; Zuilhof, H.; Sudhölter, E. J. R. *Adv. Mat.* **2000**, *12*, 1457-1460.

[2] Buriak, J. M. *Chem. Rev.* **2002**, *102*, 1271-1308.

[3] Hamers, R. J.; Coulter, S. K.; Ellison, M. D.; Hovis, J. S.; Padowitz, D. F.; Schwartz, M. P.; Greenlief, C. M.; Russell, J. N., Jr. *Acc. of Chem. Res.* **2000**, *33*, 617-624.

[4] Hamers, R. J.; Wang, Y. *Chem. Rev.* **1996**, *96*, 1261-1290.

[5] Wayner, D. D. M.; Wolkow, R. A. *J. Chem. Soc. Perkin Trans.* **2002**, *2*, 23-34

[6] Bent, S. F. *J. Phys. Chem. B* **2002**, *106*, 2830-2842.

[7] Bent, S. F. *Surface Science* **2002**, *500*, 879-903.

[8] Barriocanal, J. A.; Doren, D. J. *J. Am. Chem. Soc.* **2001**, *123*, 7340-7346.

[9] Hess, J. S.; Doren, D. J. *J. Phys. Chem. B* **2002**, *106*, 8206-8210.

[10] Mulcahy, C. P. A.; Carman, A. J.; Casey, S. M. *Surface Science* **2000**, *459*, 1-13.

[11] Wang, G. T.; Mui, C.; Musgrave, C. B.; Bent, S. F. *J. Phys. Chem. B* **1999**, *103*, 6803-6808.

[12] Hamers, R. J.; Hovis, J. S.; Greenlief, C. M.; Padowitz, D. F. *Jap. J. App. Phys.* **1999**, *38*, 3879-3887.

[13] Hamers, R. J.; Hovis, J. S.; Lee, S.; Liu, H.; Shan, J. *Physical Chemistry B* **1997**, *101*, 1489-1492.

[14] Linford, M. R.; Chidsey, C. E. D. *J. Am. Chem. Soc.* **1993**, *115*, 12631-12632.

[15] Linford, M. R. PhD. Dissertation, Stanford University, 1996.

[16] Sieval, A. B.; Opitz, R.; Maas, H. P. A.; Schoeman, M. G.; Meijer, G.; Vergeldt, F. J.; Zuilhof, H.; Sudhölter, E. J. R. *Langmuir* **2000**, *16*, 10359-10368.

[17] Sieval, A. B.; Vleeming, V.; Zuilhof, H.; Sudhölter, E. J. R. *Langmuir* **1999**, *15*, 8288-8291.

[18] Sieval, A. B.; Demirel, A. L.; Nissink, J. W. M.; Linford, M. R.; van der Maas, J. H.; de Jeu, W. H.; Zuilhof, H.; Sudhölter, E. J. R. *Langmuir* **1998**, *14*, 1759-1768.

[19] Bansal, A.; Li, X.; Lauermann, I.; Lewis, N. S. *J. Am. Chem. Soc.* **1996**, *118*, 7225-7226.

[20] Bansal, A.; Lewis, N. S. *J. Phys. Chem. B* **1998**, *102*, 1067-1070.

[21] Gurtner, C.; Wun, A. W.; Sailor, M. J. *Angew. Chem., Int. Ed. Engl.* **1999**, *38*, 1966-1968.

[22] Song, J. H.; Sailor, M. J. *J. Am. Chem. Soc.* **1998**, *120*, 2376-2381.

[23] Buriak, J. M.; Allen, M. J. *J. Am. Chem. Soc.* **1998**, *120*, 1339-1340.

[24] Buriak, J. M.; Stewart, M. P.; Geders, T. W.; Allen, M. J.; Choi, H. C.; Smith, J.; Raftery, D.; Canham, L. T. *J. Am. Chem. Soc.* **1999**, *121*, 11491-11502.

[25] Linford, M. R.; United States Patent No. 6,132,801; 2000.

[26] Jiang, G.; Niederhauser, T. L.; Linford, M. R. *Langmuir* **2004**, *20*, 1772-1774.

[27] Niederhauser, T. L.; Jiang, G.; Lua, Y.-Y.; Dorff, M. J.; Woolley, A. T.; Asplund, M. C.; Berges, D. A.; Linford, M. R. *Langmuir* **2001**, *17*, 5889-5900.

[28] Niederhauser, T. L.; Lua, Y.-Y.; Jiang, G.; Davis, S. D.; Matheson, R.; Hess, D. A.; Mowat, I. A.; Linford, M. R. *Angew. Chem., Int. Ed. Engl.* **2002**, *13*, 2353-2356.

[29] Lua, Y.-Y.; Lee, M. V.; Fillmore, W. J. J.; Matheson, R.; Sathyapalan, A.; Asplund, M. C.; Fleming, S. A.; Linford, M. R. *Angew. Chem., Int. Ed. Engl.* **2003**, *42*, 4046-4049.

[30] Lua, Y.-Y.; Niederhauser, T. L.; Wacaser, B. A.; Mowat, I. A.; Woolley, A. T.; Davis, R. C.; Fishman, H. A.; Linford, M. R. *Langmuir* **2003**, *19*, 985-988.

[31] Lu, X. *J. Am. Chem. Soc.* **2003**, *125*, 6384-6385.

[32] Mui, C.; Bent, S. F.; Musgrave, C. B. *J.Phys.Chem.A* **2000**, *104*, 2457-2462.

[33] Kim, W.; Kim, H.-N.; Lee, G. U.; Hong, Y.-K.; Lee, K.; Hwang, C.; Kim, D.-H.; Koo, J.-Y. *Phys. Rev. B* **2001**, *64*, 193313.

[34] Morikawa, Y. *Phys. Rev. B* **2001**, *63*, 033405.

[35] Mayne, A. J.; Avery, A. R.; Knall, J.; Jones, T. S.; Briggs, G. A. D.; Weinberg, W. H. *Surface Science* **1993**, *284*, 247-256.

[36] Miotto, R.; Ferraz, A. C.; Srivastava, G. P. *Phys. Rev. B* **2002**, *65*, 075401.

[37] Silvestrelli, P. L.; Toigo, F.; Ancilotto, F. J. *Chem. Phys.* **2001**, *114*, 8539.

[38] Ulman, A. *Characterization of Organic Thin Films*; Butterworth-Heinemann, 1994.

[39] Sieval, A. B.; van den Hout, B.; Zuilhof, H.; Sudhölter, E. J. R. *Langmuir* **2001**, *17*, 2172-2181.

[40] Sieval, A. B.; van den Hout, B.; Zuilhof, H.; Sudhölter, E. J. R. *Langmuir* **2000**, *16*, 2987-2990.

[41] Pei, Y.; Ma, J.; Jiang, Y. *Langmuir* **2003**, *19*, 7652-7661.

[42] Li, T.-W.; Chao, I.; Tao, Y.-T. *J.Phys.Chem.B* **1998**, *102*, 2935-2946.

[43] Bunte, S. W.; Sun, H. J. *J. Phys. Chem. B* **2000**, *104*, 2477-2489.

[44] Sun, H. J. *Phys. Chem. B* **1998**, *102*, 7338.

Chapter 3. Gas phase chemomechanical modification of silicon*

Michael V. Lee,[†] *Jody L. Richards,*[†] *Matthew R. Linford,*[†] *Sean M. Casey*[‡]

Abstract

In this work we demonstrate the gas phase chemomechanical functionalization of silicon. This work streamlines the preparation of chemomechanically modified surfaces, in comparison with previously described liquid phase modifications. Scribing was performed in the presence of ethylene, acetylene, and a control (air). X-ray photoelectron spectroscopy, wetting, and time-of-flight secondary ion mass spectrometry (scores and loadings from principal components analysis) results are consistent with expectations and with previous analysis of samples scribed under liquid alkenes and alkynes. Thermal desorption spectroscopy analysis supports the Si(100) model for scribed silicon.

Overview

Chemomechanical modification has been shown to covalently modify silicon with 1-alkenes,[1,2] 1-alkynes,[1] alcohols,[2] alkyl halides,[3] epoxides,[4] aldehydes,[5] and acid chlorides[6] in a single step. During scribing the surface oxide or hydrogen termination is mechanically removed in the presence of a chemical reagent. The scribing action induces cleavage of the silicon, producing a surface of silicon radicals.[7] The scribed silicon

---

* Reprinted with permission from Michael V. Lee, Jody L. Richards, and Matthew R. Linford "Gas Phase Chemomechanical Modification of Silicon" *Journal of Vacuum Science and Technology B: Microelectronics and Nanometer Structures* **24**, 750-755 (2006). [doi: 10.1116/1.2178369]

[†] Department of Chemistry and Biochemistry, Brigham Young University, Provo, Utah 84602

[‡] Department of Chemistry, University of Nevada, Reno, Reno, Nevada 89557

surface is likely predominantly composed of the thermodynamically favored <111>, <100>, and <110> cleavage planes. The highly studied Si(100) surface typically provides the model for scribed silicon. The surface silicon radicals rapidly react with the functional groups of the reagent, covering the surface in a manner analogous to reactions with (reconstructed) Si(100)-2x1 and Si(111)-7x7 under UHV conditions.[8 9 10 11 12]

The chemomechanical modification of silicon has some significant advantages, namely, one-step surface functionalization, open laboratory environment, and as received reagents (no degassing). Scribing is also amenable to patterning–functionalization takes place wherever a tip makes contact with a surface and (ideally) nowhere else. The method also has a few weaknesses: (1) as typically practiced, large amounts of reagents are required for monolayer scale functionalization; (2) after functionalization the excess reagent must be removed from the surface; and (3) depending on the tip and forces involved, surfaces may be rough.

In order to address the first two disadvantages of scribing, we demonstrate the chemomechanical modification of silicon with gas phase reagents. Scribing with gas phase reagents simplifies sample cleanup, introduces a range of reagents not possible with other patterning methods, and reduces the molar amount of reagent required. The process takes place by simply directing a stream of reagent gas, such as compressed ethylene, acetylene, or air (control gas), toward the silicon surface while it is being scribed.

Surface modification is confirmed by wetting, x-ray photoelectron spectroscopy (XPS), and time-of-flight secondary ion mass spectrometry (TOF-SIMS). These data, combined with thermal desorption spectroscopy (TDS) of a surface scribed under acetylene,

demonstrate the chemomechanical functionalization of silicon using a gas phase reagent and suggest a di-σ binding of unsaturated hydrocarbons on Si_{scr}, similar to the [2+2] cycloaddition-like reaction of unsaturated hydrocarbons to reconstructed Si(100)-2x1 and Si(111)-7x7.[8-12]

Experimental details

Sample preparation

Silicon (100) samples (2-6 $\Omega \cdot cm^{-1}$) were cleaned using 50:50 (v/v) 30% H_2O_2:NH_4OH (conc.) for 30 min. The samples were then rinsed with and stored under Millipore water until needed. Immediately prior to use, samples were again rinsed with Millipore water and dried with a jet of nitrogen.[1] The flow of the reagent gas was directed at the silicon surface through a 1.78 mm polyethylene tube shrouded by a glass eyedropper tube for support. The tube outlet was within a few millimeters of the tip used for scribing. A small plastic bag was placed over the scribing area in order to confine the gas in the scribing region and exclude the surrounding air. The bag did not form a seal and no additional effort was made to prevent contaminants from the air from reaching the surface. A patch was scribed using a diamond tip in a scribing apparatus that has previously been described.[1,13] In all cases a series of closely spaced lines was scribed at least once in one direction and then in the perpendicular direction to form a patch. It is believed that if a region that has been previously scribed is scribed again the resulting surface will have the same composition as the initial surface. After this process, the entire scribed surface appeared to be visibly roughened so that no unfunctionalized silicon remained.

Reagent gases

Ethylene (99.5% pure from Airgas) and compressed air (grade "D") were used as received. The acetylene (Airgas, 99.6%, dissolved in acetone) required the removal of acetone prior to use as a reagent. The acetylene was bubbled through Millipore water and then passed through a drying tube containing Drierite (anhydrous calcium sulfate) for purification. The Millipore water was replaced after scribing each sample. The gas was analyzed by gas chromatography to insure the removal of acetone. A continuous flow rate of 1500 mL/min was used for all samples. For the UHV functionalization of scribed surfaces, acetylene (99.6%, Matheson Tri-Gas, dissolved in acetone) and ethylene (95+%, Spectra Gases) were used as received. TDS calibration was performed using cis-2-butene (95%, Matheson Tri-Gas) and ammonia (99.99%, Scott Specialty Gases).

Contact angles

Samples for water contact angle measurements were produced by scribing lines with 30 μm pitch in perpendicular directions over 1 x 1 cm^2 of a silicon surface. Patches were scribed in an atmosphere of the reagent gas. The surfaces were then removed from the apparatus and blown off with a stream of nitrogen to remove loose particulates. Sessile water contact angle measurements were made with a Ramé-Hart model 100-00 contact angle goniometer. Four measurements for each reagent gas (acetylene, ethylene, and compressed air) were taken on each side of a water droplet placed upon the scribed region.

X-ray photoelectron spectroscopy (XPS) and time-of-flight secondary ion mass spectrometry (TOF-SIMS)

Samples for XPS and TOF-SIMS were produced by scribing 200 lines 3 mm long with 15 μm pitch giving a scribed area of 3x3 mm^2. Microscopic analysis showed that the whole area had been roughened. Subsequent to scribing, the debris generated was blown off with a gentle stream of nitrogen. No other cleaning of the surface was performed. XPS survey spectra and narrow scans for silicon, carbon, and oxygen were recorded for each sample.

A 500x500 μm^2 area was scanned on each sample for 400 s in the negative ion mode using the ION-TOF GmbH, TOF-SIMS IV instrument. All peak areas ± 0.2 amu around the first 100 u were extracted from the resultant spectra for each sample using the TOF-SIMS IV VER. 4.03 software. TOF-SIMS data were analyzed by principal components analysis[14] (PCA) using the PLS_TOOLBOX 3.0 by EIGENVECTOR for MATLAB. The data were preprocessed using the PLS_TOOLBOX options "normalize" and "mean center."[14] One acetylene sample was found to be an outlier and was removed; the data were reprocessed without the outlier for presentation.

Thermal desorption spectroscopy (TDS)

Samples for TDS were scribed three times in each direction over a 1x1 cm^2 area with 30 μm pitch and were afterwards dusted with a jet of nitrogen to remove loose particulates. They were then stored in an atmosphere of nitrogen for transport to Nevada where they were analyzed. In Nevada, the samples were mounted on a sample holder and introduced into a UHV chamber for TDS without any further processing. The chamber has been previously described.[15]

The samples were heated during TDS as previously described.[16] After desorption from the scribed surface and after the samples cooled, each sample was dosed under UHV conditions with 1 L of the same gas with which it had been previously scribed. Following the dosing, TDS was repeated to allow comparison of the spectra for scribed and dosed samples. The counts recorded by the quadrupole were recorded in reference to heating time. In order to correlate the heating time with temperature, each sample was dosed with water vapor,[17] ammonia,[18] ethylene,[19] acetylene,[20] and cis-2-butene.[21] The peaks from each of these known species were used to fit the heating curve to the TDS time.

Results and discussion

A material must often be probed in different ways to yield different pieces of necessary, complementary information. In this work we use wetting, XPS, TOF-SIMS, and TDS to characterize silicon surfaces that are scribed in the presence of ethylene, acetylene, and clean air. Together these methods demonstrate that silicon can be scribed in the presence of gas phase reagents and further suggest that Si_{scr} is analogous to bare reconstructed silicon.

XPS and wetting (water contact angle) measurements

XPS provides elemental analysis of surfaces. Figure 13(b) shows C1*s*/Si2*p* and O1*s*/Si2*p* ratios for the surfaces produced by scribing in the presence of ethylene, acetylene, and air. If functionalization with gas phase reagents were not possible, the gas used would not alter the composition of the surface. Figure 13(b) clearly shows a relative increase in the carbon content for surfaces prepared with ethylene and acetylene, and

higher oxygen content for surfaces scribed in compressed air. This indicates that the reagent gases do indeed react with the Si_{scr} surface.

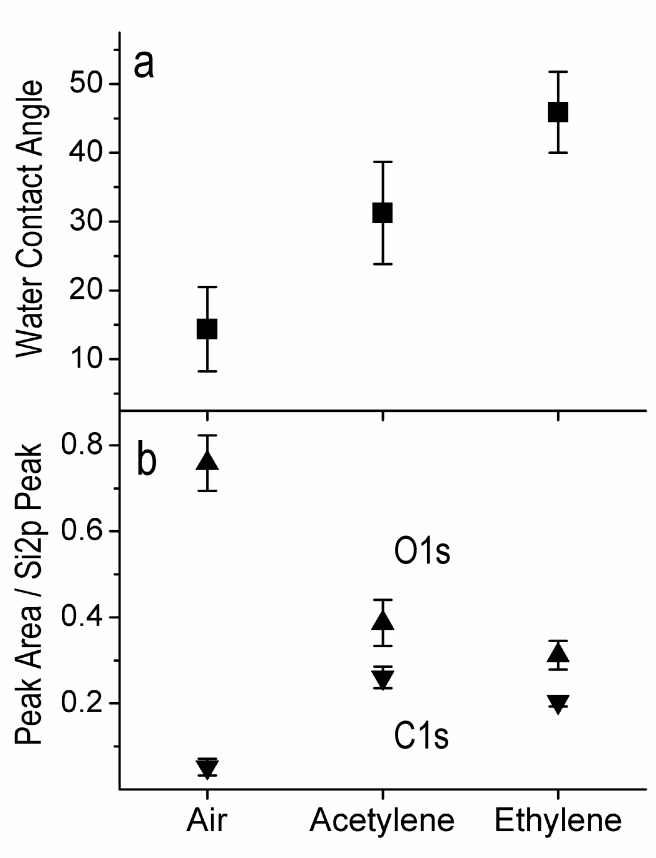

Figure 13. Water contact angles and XPS results for gas scribing silicon. (a) Sessile water contact angle measurements for surfaces scribed with ethylene, acetylene, and air. Four samples were prepared with each reagent. The contact angle was measured on both sides of the droplet with which each surface was probed. Squares indicate average values, and bars represent the range of measured values. (b) O1*s*/Si2*p* and C1*s*/Si2*p* XPS ratios for scribing in ethylene, acetylene, and air. Up triangles represent average values for O1*s*/Si2*p*, while down triangles represent average values for C1*s*/Si2*p*. Error bars represent the standard deviation of the data.

Niederhauser *et al.* published contact angle measurements and XPS data for surfaces functionalized with homologous series of 1-alkenes and 1-alkynes.[1,2] The data presented in Figure 14 and Figure 15 combine the data from surfaces prepared by scribing in ethylene and acetylene with the previously published data. These results correlate well and suggest that the reaction of double and triple bonds with the scribed surface is the same for both liquid and gaseous reagents.

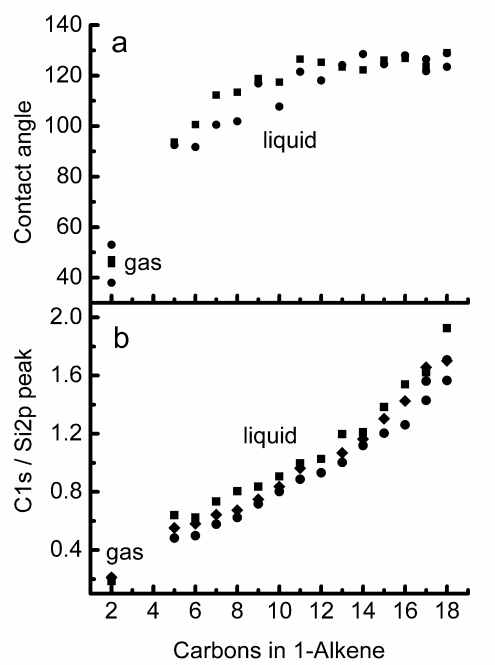

Figure 14. Comparison of contact angle and XPS measurements for liquid and gas 1-alkene scribed surfaces. (a) Water contact angles on silicon surfaces scribed with 1-alkenes. (b) XPS C(1s)/Si(2p) ratios for silicon scribed under liquid 1-alkenes and ethylene. Symbols for 5-18 carbon chains (previously published data) represent functionalization using liquid reagents, while those with two carbons (this article) represent ethylene.

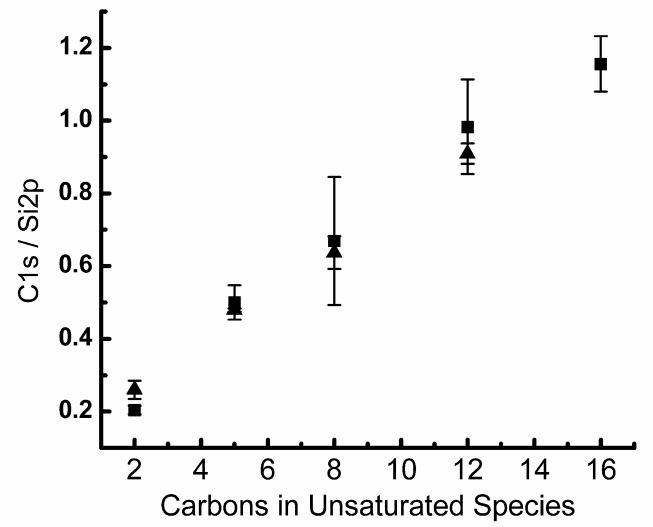

Figure 15. Comparison of past XPS data for 1-alkenes and 1-alkynes with gas phase scribing. Squares represent 1-alkenes while triangles represent 1-alkynes. Symbols for two carbon chains (this article) represent functionalization using ethylene and acetylene gaseous reagents, while symbols for 5, 8, 12, and 16 carbon chains (previously published data) represent functionalization with liquid 1-alkenes and 1-alkynes.

Contact angle measurements probe surface free energies of materials; hydrophobic surfaces have higher water contact angles than more hydrophilic surfaces. The bare silicon surface that is created during scribing is expected to react readily with oxygen to form a hydrophilic oxide layer, or with ethylene or acetylene to form tethered organic species. If ethylene and acetylene adsorb onto Si_{scr} as they do on Si(100)-2x1 or Si(111)-7x7 each molecule should be tethered through a pair of carbon-silicon bonds. Hence, for equal coverages, one would expect that a silicon surface with tethered acetylene molecules would be more hydrophilic than that scribed with ethylene because of the polarizable carbon-carbon double bond of a bound acetylene molecule. As expected, the surface scribed under air is the most hydrophilic, followed by the surface made from acetylene [see Figure 13(a)]. The spread in the data in Figure 13(a) is most likely due to the roughness of the surfaces. XPS and wetting provide the first evidence of functionalization of scribed silicon by gaseous reagents demonstrate similar surfaces to those produced by liquid reagents and exhibit properties consistent with binding analogous to reconstructed silicon in UHV.

TOF-SIMS analysis

TOF-SIMS typically provides valuable chemical information about materials in the form of highly characteristic ions. An important method of extracting chemical information from the complex spectra that are often produced by TOF-SIMS is PCA, i.e., PCA is used to find the variation in the data.[14] In PCA of TOF-SIMS data, the areas of the different peaks at different masses (the variables) are usually normalized and then mean centered. PCA can then be viewed as "plotting" the spectra as single points in a hyperspace of these variables and as rotating the coordinate system to account for the

maximum variation in the data. The first principal component (PC1) is the axis that accounts for the largest fraction of the variation in the data. The second principal component (PC2) is the axis that accounts for the next largest fraction of the variation, etc. The projections of the data points onto the PCs are called scores. The contributions of the original axes to the PCs are called loadings.

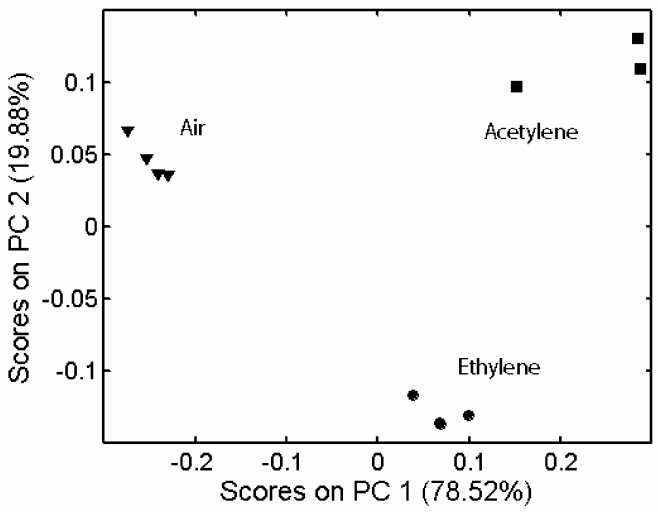

Figure 16. PCA Score plot of TOF-SIMS spectra of gas phase scribed samples. Ethylene, acetylene, and compressed air samples are represented by circles, squares, and triangles, respectively. The amount of variation in the data accounted for by each principal component is given in parentheses. One sample for acetylene was found to be a significant outlier and was omitted.

Accordingly, surfaces produced by scribing silicon under ethylene, acetylene, and air were probed with TOF-SIMS and the resulting negative ion spectra were analyzed using PCA. A score plot for the projections of the data onto PC1 and PC2 is shown in Figure 16. The separation between the samples on the score plot graphically represents the chemical differences between them. PC1, which accounts for more than 80% of the chemical variation in the data, separates the compressed air samples from those scribed under hydrocarbons. PC2, describing the next most significant variation in the data, cleanly separates the surfaces scribed under ethylene and acetylene. This indicates that the samples from the two hydrocarbon reagents create functionalized surfaces that are

chemically distinct, yet more similar to each other than to the surfaces functionalized in an atmosphere of compressed air.

Complementary to the score plots are the loadings of the PCs, which represent the contribution of each variable to each principal component. Positive (or negative) loadings correlate with positive (or negative) scores on the related score plot and larger absolute values for loadings indicate greater significance. The presence of C_2H^- and C_2^- as major contributors for PC1 suggests that ethylene and acetylene chemisorb without decomposing and that upon ion bombardment a significant fraction of the molecules are ejected molecularly. Notably O^- represents most of the negative loading for PC1, suggesting oxide formation on silicon scribed under compressed air. Production of negative ions from electronegative species on an electropositive substrate should be favorable; it should come as a small surprise that this matrix effect leads to Cl^- formation even though chlorine appears to be present at trace levels, *i.e.*, chlorine is not detected in XPS survey scans of the surfaces.

PC2 accounts for the differences between silicon scribed in the presence of ethylene and acetylene. Table I shows the ten peaks that make the largest contributions to PC2. Acetylene molecularly bound to the silicon surface through two carbon-silicon bonds would retain its double bond. A double bond between the carbons would make them less likely to dissociate and produce strong carbon-hydrogen bonds. This would explain the prominence of the C_2H^- peak in PC2 and would give validity to the assumption made in explaining the lower water contact angle for acetylene compared to ethylene. The H^- peak on PC2, as well as the O^- peak compared to the OH^-, peak suggests that the negatively

scored samples on PC2 (ethylene) have more hydrogen than the positively scored samples (acetylene).

Table 1 PCA loadings for TOF-SIMS peaks for each PC for gas phase $Si_{scr.}$ Peaks from negative ion TOF-SIMS spectra. Positive loadings for a peak indicate contribution to samples with positive scores for that principal component. Larger absolute value loading indicates more significant correlation.

Principal component 1			Principal component 2		
Peak (*m*/*z*)	Loadings	Identity	Peak (*m*/*z*)	Loadings	Identity
25	0.6411	C_2H^-	25	0.6896	C_2H^-
16	-0.5067	O^-	1	-0.5095	H^-
1	0.4058	H^-	17	-0.3143	OH^-
35	0.2466	Cl^-	16	0.2284	O^-
17	0.1560	OH^-	35	-0.1838	Cl^-
24	0.1274	C_2^-	61	-0.1487	SiO_2H^-
13	0.1155	CH^-	77	0.1333	SiO_3H^-
41	0.1011	$SiCH^-$	24	0.1314	C_2^-
77	-0.1000	SiO_3H^-	37	-0.0562	Cl^-
61	0.0900	SiO_2H^-	45	-0.0549	$SiOH^-$

TDS analysis

TDS scans for surfaces functionalized with acetylene are shown in Figure 17. Figure 17(a) shows dosed Si(100)-2x1 and includes peaks for desorption of molecular acetylene and hydrogen that are consistent with literature values. The middle spectra are of silicon scribed in the presence of acetylene, while the bottom spectra are of the scribed surface following both TDS and subsequent dosing with acetylene. The spectra were calibrated by subsequent dosing with characteristic molecules (see Experimental Details). The calibration peaks for the Si(100) sample in (a) were measured on the same sample following the recording of the data in (a). The spectra in (b) and (c) were calibrated by measuring dosed peaks for the scribed sample subsequent to taking the data in both (b) and (c).

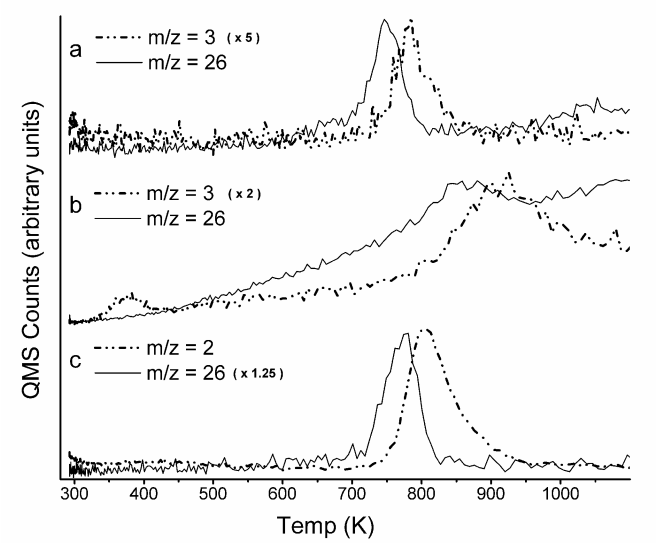

Figure 17. TDS spectra of acetylene on silicon (a) Desorption spectra for HD (*m*/*z*=3) and C_2H_2 (*m*/*z* =26) from reconstructed Si(100)-2x1 dosed with acetylene. (b) Desorption spectra for HD (*m*/*z* =3) and C_2H_2 (*m*/*z* =26) from silicon scribed in the presence of acetylene. (c) Desorption spectra for H_2 (*m*/*z* =2) and C_2H_2 (*m*/*z* =26) from a scribed silicon surface after annealing and dosing with acetylene. In each spectrum the solid lines represent the acetylene parent ion. The dashed lines in spectra (a), (b), and (c) represent molecular hydrogen desorption. The spectra have temperature uncertainties of ±20 K and ±45 K for (a) and (c), respectively. The temperature uncertainty for (b) is unknown. The rise in counts in (b) is due to rising baseline counts. The samples were heated at about 10 K/s.

Scribed silicon is believed to be composed of multiple silicon crystal faces with the preferential cleavage planes <111>, <100>, and <110> representing the majority of the surfaces with various other planes representing the interface between them. Desorption of species bound to these various faces is consistent with the broadening seen in (b). Annealing narrows the desorption peaks as seen in (c).

We have reason to believe that the temperature calibration is incorrect in Figure 17(b). The sample had a native oxide on the surface when TDS was performed, but the oxide was absent during the calibration. The higher emissivity of the native oxide layer would result in a shift in the temperature calibration. The supposition that the temperature is shifted is supported by the hydrogen peaks desorbed from the sample in (b). Desorption of hydrogen from silicon surfaces has been well studied, including Si(100), [22,23] Si(111),[22,24] and amorphous,[25] and porous[26,27] silicon. Two peaks are typically found, the

lower temperature peak between 600 and 650 K and the higher temperature peak between 700 and 800 K. The generality of these two peaks suggests that the peak found in Figure 17(b) at 900 K is actually one of these two hydrogen desorption peaks. The higher temperature peak, the more prominent of the two for Si(100), Si(111), amorphous silicon, and likely scribed silicon, is due to desorption of hydrogen from monohydride surface species. The lower temperature peak is due to hydrogen desorption from dihydride moieties and accompanies desorption of Si_xH_y species from surfaces such as porous silicon that are rich in hydrogen. The absence of a SiH^+ (m/z=29) peak (data not shown) indicates that the surfaces in Figure 17 are not rich in SiH_2 and SiH_3 and that the hydrogen peak for each surface is the high temperature peak found between 700 and 800 K. The small peak at 375 K in (b) also supports the proposed temperature shift. As the sample heating begins, physisorbed species desorb from the sample and sample holder,[24] as is seen in the elevated hydrogen signal at 300 K in Figure 17(a) and Figure 17(c); slower heating would shift this desorption to an apparent higher temperature as well, producing the peak at 375 K.

If the shift is corrected by aligning the hydrogen desorption peaks as shown in Figure 18, the acetylene desorption peaks from all three spectra are also quite well aligned; this indicates that chemomechanically functionalized acetylene desorbs from scribed silicon between about 700 and 800 K, similar to the temperature at which dosed acetylene desorbs from Si(100)-2x1 and annealed Si_{scr}. A hydrocarbon bound to silicon by only a single Si-C bond desorbs from Si(100) at below 600 K,[28] far below the temperature of desorption of acetylene from Si_{scr}; this suggests that acetylene indeed binds to Si_{scr}

through two Si-C σ bonds, similar to the binding of unsaturated hydrocarbons to Si(100)-2x1 and Si(111)-7x7.

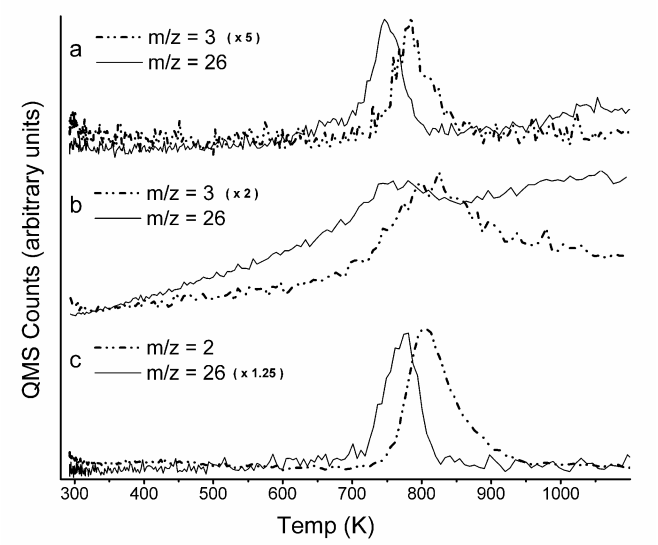

Figure 18. TDS spectra of acetylene on silicon after aligning the hydrogen peaks (a) Desorption spectra for HD (*m*/*z* =3) and C_2H_2 (*m*/*z* =26) from reconstructed Si(100)-2x1 dosed with acetylene. (b) Desorption spectra for HD (*m*/*z* =3) and C_2H_2 (*m*/*z* =26) from silicon scribed in the presence of acetylene. (c) Desorption spectra for H_2 (*m*/*z* =2) and C_2H_2 (*m*/*z* =26) from a scribed silicon surface after annealing and dosing with acetylene. In each spectrum the solid lines represent the acetylene parent ion. The dashed lines in spectra a, b, and c represent molecular hydrogen desorption. The spectra have temperature uncertainties of ±20 K and ±45 K for (a) and (c), respectively. The temperature uncertainty for (b) is unknown. The rise in counts in (b) is due to rising baseline counts. The samples were heated at about 10 K/s.

Conclusion

Chemomechanical surface modification is a straightforward method for simultaneously functionalizing and patterning silicon. We have demonstrated that the functionalization is not limited to condensed phase reagents. Acetylene and ethylene appear to react with Si_{scr} in the same manner that liquid 1-alkenes and 1-alkynes react with Si_{scr}. We provide compelling evidence that acetylene binds to Si_{scr} through two Si-C bonds in a manner analogous to the [2+2] cycloaddition-like binding of unsaturated hydrocarbons to Si(100)-2x1 and Si(111)-7x7. Gaseous reactants allow a wider scope of reagents for functionalization, smaller molar amounts of reagent, easier sample cleaning, and more direct comparison with UHV chemistry.

Acknowledgments

The authors thank the Petroleum Research Fund, the College of Physical and Mathematical Sciences at the Brigham Young University, and the University of Nevada, Reno for support.

Attribution

I initiated the project with the sanction of Dr. Linford. Jody Richards assisted me in the development of the system to confine the gases to the scribed area and assisted in some of the scribing and instrumental analysis. I prepared and analyzed most of the samples. I performed the principal components analysis of the data and, with the assistance of Dr. Linford, interpreted the results. Dr. Casey performed the thermal desorption spectroscopy, UHV dosing of wafers, and calibration of the samples with some assistance from myself.

---

[1] Niederhauser, T. L.; Jiang, G.; Lua, Y.-Y.; Dorff, M. J.; Woolley, A. T.; Asplund, M. C.; Berges, D. A.; Linford, M. R. *Langmuir* **2001**, *17*, 5889.

[2] Niederhauser, T. L.; Lua, Y.-Y.; Jiang, G.; Davis, S. D.; Matheson, R.; Hess, D. A.; Mowat, I. A.; Linford, M. R. *Angew. Chem., Int. Ed. Engl.* **2002**, *13*, 2353.

[3] Niederhauser, T. L.; Lua, Y.-Y.; Sun, Y.; Jiang, G.; Strossman, G. S.; Pianetta, P.; Linford, M. R. *Chemistry of Materials* **2002**, *14*, 27.

[4] Lua, Y.-Y.; Lee, M. V.; Fillmore, W. J. J.; Matheson, R.; Sathyapalan, A.; Asplund, M. C.; Fleming, S. A.; and Linford, M. R. *Angew. Chem. Int. Ed.* **2003**, *42*, 4046.

[5] Lua, Y.-Y.; Fillmore, W. J. J.; Linford, M. R. *Appl. Surf. Sci.* **2004**, *231-232*, 323.

[6] Lua, Y.-Y.; Fillmore, W. J. J.; Yang, L.; Lee, M. V.; Savage, P. B.; Asplund, M. C.; Linford, M. R. *Langmuir* **2005**, *21*, 2093.

[7] Jiang, G.; Niederhauser, T. L.; Fleming, S. A.; Asplund, M. C.; Linford, M. R. *Langmuir* **2004**, *20*, 1772.

[8] Hamers, R. J.; Wang, Y. *Chemical Reviews* **1996**, *96*, 1261.

[9] Buriak, J. M. *Chemical Communications* **1999**, *12*, 1051.

[10] Buriak, J. M. *Chemical Reviews* **2002**, *102*, 1271.

[11] Bent, S. F. *J. Phys. Chem. B* **2002**, *106*, 2830.

[12] Bent, S. F. *Surface Science* **2002**, *500*, 879.

[13] Cannon, B. R.; Lillian, T. D.; Howell, L. L.; Magleby, S. P.; Niederhauser, T. L.; Linford, M. R. *Precision Engineering* **2005**, *29*, 86-94.

[14] Brereton, R. G. *Chemometrics. Data Analsis for the Laboratory and Chemical Plant* (John Wiley & Sons, Ltd., Chichester, 2003)

[15] Mulcahy, C. P. A.; Carman, A. J.; Casey, S. M. *Surface Science* **2000**, *459*, 1.

[16] Zhang, L.; Carman, A. J.; Casey, S. M. *J. Phys. Chem. B* **2003**, *107*, 8424.

[17] Flowers, M. C.; Jonathan, N. B. H.; Morris, A.; Wright, S. *Surface Science* **1996**, *351*, 87.

[18] Dresser, M. J.; Taylor, P. A.; Wallace, R. M.; Choyke, W. J.; Yates, J. T., Jr., *Surface Science* **1989**, *218*, 75.

[19] Clemen, L.; Wallace, R. M.; Taylor, P. A.; Dresser, M. J.; Choyke, W. J.; Weinberg, W. H.; Yates, J. T., Jr., *Surface Science* **1992**, *268*, 205.

[20] Taylor, P. A.; Wallace, R. M.; Cheng, C.-C.; Weinberg, W. H.; Dresser, M. J.; Choyke, W. J.; Yates, J. T., Jr., *J. Am. Chem. Soc.* **1992**, *114*, 6754.

[21] Kiskinova M.; Yates, J. T., Jr., *Surface Science* **1995**, *325*, 1.

[22] Niwano, M.; Terashi, M.; Kuge, J. *Surf. Sci.* **1999**, *420*, 6-16.

[23] Gates, S. M.; Kunz, R. R.; Greenlief, C. M. *Surf. Sci.* **1989**, *207*, 364-384.

[24] Schulze, G.; Henzler, M. *Surf. Sci.* **1983**, *124*, 336-350.

[25] Farjas, J.; Das, D.; Fort, J.; Roura, P.; Bertran, E. *Phys. Rev. B* **2002**, *65*, 115403.

[26] Martin, P.; Fernandez, J. F.; Sanchez, C. R. *Phys. Stat. Sol.* **2000**, *182*, 255.

[27] Martin, P.; Fernandez, J. F.; Sanchez, C. *Materials Science and Engineering B* **2004**, *108*, 166-170.

[28] Bulanin, K. M.; Shah, A. G.; Fitzgerald, D. R.; Doren, D. J.; Teplyakov, A. V. *J. Phys. Chem. B* **2002**, *106*, 7286-7289.

Chapter 4. Chemomechanical nanolithography: nanografting on silicon and factors impacting linewidth*

Michael V. Lee,[†] Melinda Tonks Hoffman,[‡] Katherine Barnett,[‡] John-Mark Geiss,[‡] Vincent S. Smentkowski,[§] Matthew R. Linford,[†] and Robert C. Davis[‡]

Abstract

We present a two-fold extension of previous work on atomic force microscopy-based chemomechanical functionalization: (1) chemomechanical nanografting, which extends the chemomechanical functionalization to a more stable initial surface, and (2) linewidth studies that show the impact of force and atomic force microscopy probe tip wear on patterning resolution. Alkene, alcohol, and alkyl halide molecules were nanografted to silicon and imaged with *in situ* atomic force microscopy, with time-of-flight secondary ion mass spectrometry analyzed using Automated eXpert Spectrum Image Analysis, and with scanning electron microscopy. Chemomechanical nanografting demonstrated linewidths down to 50 nm. Lines written on hydrogen-terminated silicon were used to explore the impact of tip radius and tip wear on linewidth when using Si_3N_4 coated tips.

---

* Reprinted in full with permission from Michael V. Lee, Melinda Tonks Hoffman, Katherine Barnett, John-Mark Geiss, Vincent S. Smentkowski, Matthew R. Linford, and Robert C. Davis "Chemomechanical Nanolithography: Nanografting on Silicon and Factors Impacting Linewidth" *Journal of Nanoscience and Nanotechnology* **6**, 1639-1643 (2006). [doi: 10.1166/jnn.2006.220]

[†] Department of Chemistry and Biochemistry, Brigham Young University, Provo, UT 84602

[‡] Department of Physics and Astronomy, Brigham Young University, Provo, UT 84602

[§] Global Research Center, General Electric, Niskayuna, New York 12309

Overview

Chemomechanical functionalization of silicon was first demonstrated by grinding silicon in an alkene.[1] Linford and coworkers extended the method to patterning flat semiconductor surfaces by scribing through oxide on silicon wafers to reach underlying silicon while the surface was covered with neat liquid alkenes,[2,3] alkynes,[2] alcohols,[3] aldehydes,[4] alkyl halides,[5] epoxides,[6] and acid chlorides,[7] each of which is believed to react with surface silicon radicals produced by the scribing action.[8] Chemomechanical functionalization produces monolayers bound by strong Si-C or Si-O bonds. Monolayers bound through Si-C bonds are stable even in boiling *m*-xylene[2] and boiling 0.1 M sulfuric acid.[9]

Atomic force microscopy (AFM) probe tips have been used to chemomechanically functionalize hydrogen-terminated silicon (Si(111)-H), creating high resolution features (below 30 nm)[10] comparable to other nanoscale scanning probe lithography techniques.[11,12,13,14] However, the Si(111)-H must be patterned shortly after preparation since oxide forms on the surface inhibiting chemomechanical activation of the surface.

Berrie and coworkers recently demonstrated patterning of a more stable silicon surface using a nanoshaving process on alkyl-terminated silicon. In this process, an AFM probe tip scrapes covalently bound dodecyl chains off the silicon substrate.[15] Nanografting, closely related to nanoshaving, removes a protective molecule from a surface while a reactive molecule is present; the reactive molecule binds in the exposed region, forming a tightly packed monolayer. Liu and coworkers demonstrated the nanografting process on gold. They shaved a decane thiol monolayer from a gold surface, shearing the weak Au-S bond and baring the gold surface in the presence of octadecane thiol that assembled on the exposed surface.[16] The nanografting approach has been expanded to include

nanografting bifunctional molecules that are used as handles for binding other chemicals and biological molecules.[14,17]

In this work we show nanografting of alkene, alcohol, and alkyl halide reagents to silicon through a protective monolayer derived by reacting 1-octene with a Si(111)-H surface (Si(111)-C_8).[18] Chemomechanical nanografting of alkyl-monolayer functionalized silicon extends chemomechanical functionalization to a primary surface that is stable for weeks rather than ca. 30 minutes with hydrogen-terminated silicon. An initial surface was also prepared by attaching an alcohol to Si(111)-H chemomechanically by AFM, rather than chemically. This alcohol functionalized surface was then used for subsequent nanografting of an alkene to the surface. Lines nanografted through alkyl monolayers resulted in linewidths down to 50 nm.

A significant issue in chemomechanical patterning, whether on Si(111)-H or nanografting on Si(111)-C_8, is achievable linewidth and the effect of tip force and tip radius on the linewidth.[9] On these surfaces, mechanical abrasion can significantly increase tip size. To study the dependence of linewidth on applied force and tip wear; lines were chemomechanically written with Si_3N_4 coated silicon tips on Si(111)-H. There was a dependence of linewidth on force, however, for Si_3N_4 coated probes; wear was generally the most significant factor determining linewidth.

Experimental

Chemomechanical functionalization sample preparation

Si(111) samples were cleaned by immersion in 3:7 ratio H_2O_2 (30%) : H_2SO_4 (95%) solution for ten minutes at 100-130 ºC and then rinsed with Milli-Q water and dried with dry nitrogen. To remove the oxide and hydrogen-terminate the silicon surface, the

samples were immersed in either 40% NH_4F, aq, for seven minutes or 5% HF, aq, for ten minutes. Samples were rinsed with Milli-Q water and dried with dry nitrogen. Samples prepared for patterning on Si(111)-H were taken to the AFM directly following hydrogen-termination of the silicon. Octadecene (1-octadecene, 97%, Fluka) and dibromooctane (1,8-dibromooctane, 98%, Aldrich) were used to create lines on Si(111)-H for wear studies and perfluorinated heptanol (1H,1H,7H-dodecafluoroheptanol, 97%, Acros) was used to chemomechanically functionalize an area on Si(111)-H for later use in nanografting.

Chemomechanical nanografting sample preparation

Immediately following hydrogen-termination, samples prepared for nanografting were alkylated by immersion in refluxing, degassed 1-octene (98%, Aldrich) for four hours.[18] The samples were then rinsed with ethanol (100%), dichloromethane (spectrograde), and Milli-Q water. Samples were stored under Milli-Q water until use for nanografting. Reagents nanografted onto silicon include: perfluorinated decene (3,3,4,4,5,5,6,6,7,7,8,8,9,9,10,10,10-heptadecafluoro-1-decene, 99%, Aldrich), decadiene (1,9-decadiene, 96%, Aldrich), decene (1-decene, 99%, Aldrich), perfluorinated heptanol, perfluorinated iodooctane (1,1,1,2,2,3,3,4,4,5,5,6,6,-tridecafluoro-1-iodooctane, 96%, Aldrich), and dibromooctane. All reagents were used as received.

AFM chemomechanical patterning

High-k Si_3N_4 coated tips (NSC11/Si3N4/AlBS, Mikromasch) were loaded on a fluid cell which was then mounted on the AFM (Dimension 3100 with Nanoscope III 4.43r8 software including Nanoscript, Digital Instruments). The AFM was operated in contact

mode. Square areas were nanografted for TOF-SIMS and SEM analysis by increasing the deflection setpoint. Using a script written in the instrument macro language (Nanoscript), lines were either chemomechanically created on Si(111)-H or chemomechanically nanografted on Si(111)-C_8. After chemomechanical modification, samples were rinsed with spectrograde acetone, rinsed with Milli-Q water, and dried under a gentle flow of dry, particle-free nitrogen.

Sample analysis

In situ AFM-height and lateral force microscopy (LFM) images were obtained before and after patterning; TOF-SIMS and SEM images were obtained after patterning. After rinsing and drying, modified Si(111)-C_8 samples were imaged by TOF-SIMS (TOF-SIMS IV, ION-TOF GmbH). The TOF-SIMS data were analyzed by manually selecting peaks indicative of the sample surface species and also by Automated eXpert Spectrum Image Analysis (AXSIA),[19] a multivariate statistical analysis technique.[20,21] Prior to imaging by SEM (XL 30 FEG ESEM, Philips), samples with nanografted decadiene were immersed overnight in a 1.5% (wt.) osmium tetroxide (Aldrich, 99.8%) solution in Milli-Q water to increase SEM contrast. While a significant amount of hydrolysis of the osmate ester most likely occurred, XPS showed that osmium preferentially deposited on macroscale decadiene-derived surfaces compared to decene-derived surfaces for overnight exposure. SEM contrast is expected from the preferential deposition. AFM probes and lines on Si(111)-H were imaged directly by SEM (XL 30 S-FEG SEM with in-lens detector, Philips).

Linewidth measurements and correlation calculations

The lines created on Si(111)-H were made in the same manner as the nanografted lines. A single tip was used to create a series of 50 lines chemomechanically functionalized at 10 different forces in random order. The experiment was performed twice. These samples were then examined by *in situ* AFM-height and LFM and SEM (S-FEG). The images of the lines were interpreted by Scion Image for Windows Beta 4.0.2 (Scion Corp.) and the heights parallel to the lines were averaged. The averaged values were imported into Origin 6.1 (OriginLab Corp.) and fitted to Gaussian curves to determine the FWHM linewidth.

For each series of lines created with the same tip the correlation $\rho_{x,y}$ between linewidth and line number, and also between linewidth and applied force, were calculated using the following relation:

$$\rho_{x,y} = \frac{\frac{1}{n}\sum_{1}^{n}\left(x_j - \mu_x\right)\left(y_j - \mu_y\right)}{\sigma_x \cdot \sigma_y}$$

Where n is the number of lines and x_j in the linewidth. When calculating wear correlations, y_i is the line number. When calculating force correlations, y_i is the applied force. μ and σ are respectively the means and standard deviations of the *x* and *y* values.

Results and discussion

Chemomechanical nanografting

Alkenes, alcohols, and alkyl halides were chemomechanically nanografted to silicon as shown by *in situ* AFM-height, LFM, SEM, and TOF-SIMS imaging (Figure 19). Micron sized areas were nanografted so that lower spatial resolution TOF-SIMS analysis could

be used to compare similar samples to those analyzed by AFM and SEM. Lines were nanografted to demonstrate that the resolution achievable by chemomechanical nanografting is similar to that achievable by chemomechanical functionalization with an AFM tip.

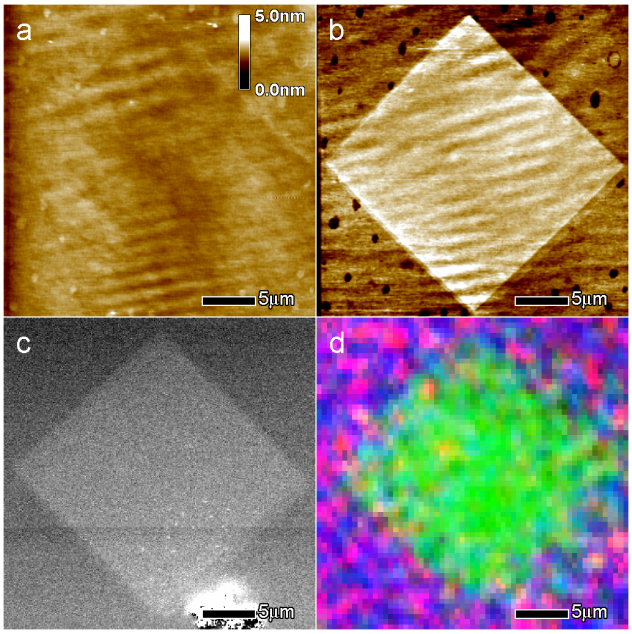

Figure 19. AFM, TOF-SIMS, and SEM of 20x20 µm squares (45º) nanografted on silicon displacing an alkyl monolayer, Si(111)-C_8. Images are 30x30 µm. *In situ* (a) height and (b) lateral force images (scan angle 90º) of a nanografted 1-decene square. Optical interference, likely from the fluid cell, was removed from (a) and (b) with the FFT function in the AFM software; residual noise is apparent in the images. (c) SEM secondary electron image of a square of nanografted 1,9-decadiene after exposure to osmium tetroxide. (d) Composite RGB representation of TOF-SIMS negative ion scans of a nanografted perfluorinated heptanol square. Red represents hydrogen; green, fluorine; and blue, hydrocarbon counts. Red, green, and blue were adjusted independently for maximum contrast. The TOF-SIMS was operated in bunch mode, resulting in lower resolution in this image compared with AFM and SEM; here TOF-SIMS is used to confirm the change in the chemical nature of the box rather than to define the functionalized area. Reprinted with permission from Michael V. Lee, Melinda Tonks Hoffman, Katherine Barnett, John-Mark Geiss, Vincent S. Smentkowski, Matthew R. Linford, and Robert C. Davis "Chemomechanical Nanolithography: Nanografting on Silicon and Factors Impacting Linewidth" *Journal of Nanoscience and Nanotechnology* **6**, 1639-1643 (2006). [doi: 10.1166/jnn.2006.220] Copyright © 2006 American Scientific Publishers, http://www.aspbs.com.

The height difference between the nanografted region and the eight carbon passivating monolayer in Figure 19a was <3 Å, yet the same region by LFM in Figure 19b shows large contrast between the two chemically distinct regions. The similarity in height indicates that a monolayer or less of silicon was removed, much less than the 2 to 15

nanometers in the silicon nanoshaving work by Berrie and coworkers.[15] Nanografting decadiene on the Si(111)-C_8 surface created a region terminated with double bonds; exposing this alkyl layer to osmium tetraoxide allowed SEM (Figure 19c) to visualize the nanografted decadiene pattern. Lines with widths down to 50 nm were nanografted on Si(111)-C_8 using the scripting program.

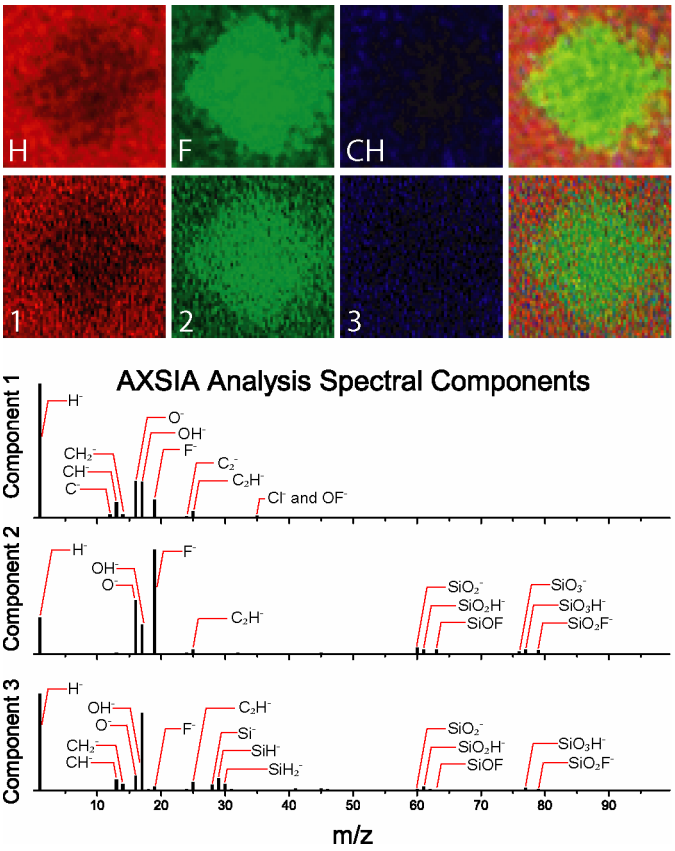

Figure 20. Univariate and AXSIA (multivariate) Analysis of negative ion TOF-SIMS raw data from a square of perfluorinated heptanol nanografted through Si(111)-C_8. The univariate analysis, shown on the top row of the Figure, extracted the hydrogen peak (H), represented by red, the fluorine peak (F), represented by green, and the hydrocarbon peaks (CH), represented by blue. The AXSIA analysis produced three similar components: Component 1, represented by red, predominates where nanografting was not performed and is indicative of hydrocarbon species. Component 2, represented by green, is present primarily where perfluorinated heptanol was nanografted and accounts for fluorine and oxygen species. Component 3 is represented by blue. Both analyses produce similar results with the fluorine peak representative of Component 2 and the hydrogen and hydrocarbon peaks representative of Components 1 and 3. As in Figure 19b, low spatial resolution resulted in noisy images. The images were taken in "bunch" mode. Spot size is *ca.* 3 μm and exceeds the pixel size in these images. Reprinted with permission from Michael V. Lee, Melinda Tonks Hoffman, Katherine Barnett, John-Mark Geiss, Vincent S. Smentkowski, Matthew R. Linford, and Robert C. Davis "Chemomechanical Nanolithography: Nanografting on Silicon and Factors Impacting Linewidth" *Journal of Nanoscience and Nanotechnology* **6**, 1639-1643 (2006). [doi: 10.1166/jnn.2006.220] Copyright © 2006 American Scientific Publishers, http://www.aspbs.com.

AXSIA analysis of TOF-SIMS spectra

TOF-SIMS was used to determine the chemical functionalization of the nanografted regions. The TOF-SIMS image in Figure 19d is of a perfluorinated heptanol square nanografted in the place of the 1-octene derived layer. The nanografted region shows increased fluorine (F^-) and suppressed hydrogen (H^-) and hydrocarbon (CH^-) peaks compared to the surrounding passivating layer. The prominence of fluorine and lack of hydrogen in the nanografted region supports the proposed replacement of the original eight chain hydrocarbon by the chemically distinct, fluorine-rich decyl groups.

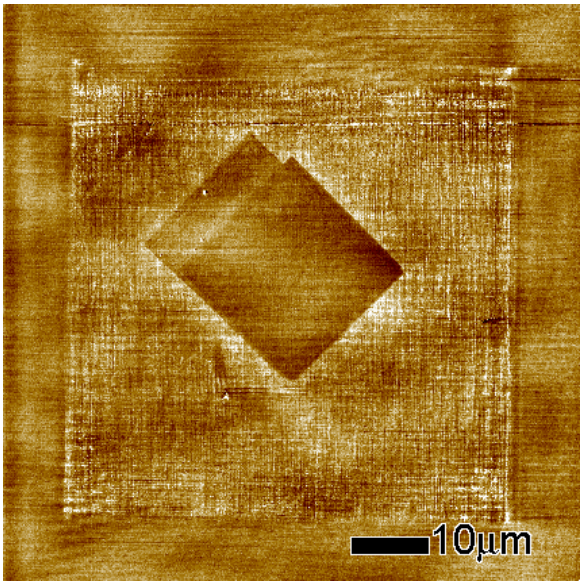

Figure 21. LFM image of chemomechanically nanografted area within a chemomechanically functionalized box. A 60 µm square box of perfluorinated heptanol was functionalized on Si(111)-H. The excess reagent was cleaned from the surface and from the tip before both were returned to the AFM. The box was found again and an area 20 µm x 25 µm of 1,9-decadiene was nanografted in the center. The area was grafted at 45º and 135º; a higher scanning speed (200 µm/s) was used in one direction than the other (80 µm/s), leading to the irregular shape of the nanografted area. Reprinted with permission from Michael V. Lee, Melinda Tonks Hoffman, Katherine Barnett, John-Mark Geiss, Vincent S. Smentkowski, Matthew R. Linford, and Robert C. Davis "Chemomechanical Nanolithography: Nanografting on Silicon and Factors Impacting Linewidth" *Journal of Nanoscience and Nanotechnology* **6**, 1639-1643 (2006). [doi: 10.1166/jnn.2006.220] Copyright © 2006 American Scientific Publishers, http://www.aspbs.com.

This univariate analysis is compared with the multivariate AXSIA-derived analysis (images and spectra) in Figure 20. The multivariate approach confirms the separation shown by manual peak selection. Spectrum 2, concentrated in the area of the nanografted

box, is composed primarily of fluorine and oxygen peaks. The H^-, C^-, CH^-, CH_2^-, C_2^-, and C_2H^- peaks are found primarily in Spectra 1 and 3 which are found in the region surrounding the nanografted box.

Chemomechanical nanografting read-write

In addition to the chemically prepared surfaces used as the passivating layer for nanografting, a surface prepared chemomechanically by AFM on Si(111)-H was also used for nanografting. An area on a Si(111)-H sample was mechanically scribed with an AFM tip while the surface was covered with perfluorinated heptanol, producing a heptanol monolayer surface for nanografting. After rinsing the sample surface and the AFM probe tip, the same tip was used to nanograft an alkene in the center of the alcohol functionalized region, Figure 21. This demonstrates the versatility of chemomechanical patterning in that multiple chemicals can be nanografted onto a single surface and a previously patterned layer can be "rewritten" with a different functional group.

Tip wear studies

Lines written chemomechanically on Si(111)-H for wear studies (see Figure 22) revealed that the durability of the nitride-coated tips varied greatly from tip to tip and that linewidth depended both on wear and the force applied. The calculated correlations between linewidth and the order in which the lines were created were 0.86 for the first tip (Figure 22d) and 0.67 for the second tip. The correlations relating force and linewidth were 0.10 (insignificant), and 0.35 for the first and second tips respectively. These results show the predominance of tip wear (for Si_3N_4 coated silicon tips) on the resulting linewidth. The large difference in the wear characteristics of these two tips was

representative of the variability in scribing performance seen tip to tip. More durable tip materials like diamond are clearly desirable for high resolution patterning on silicon.[22]

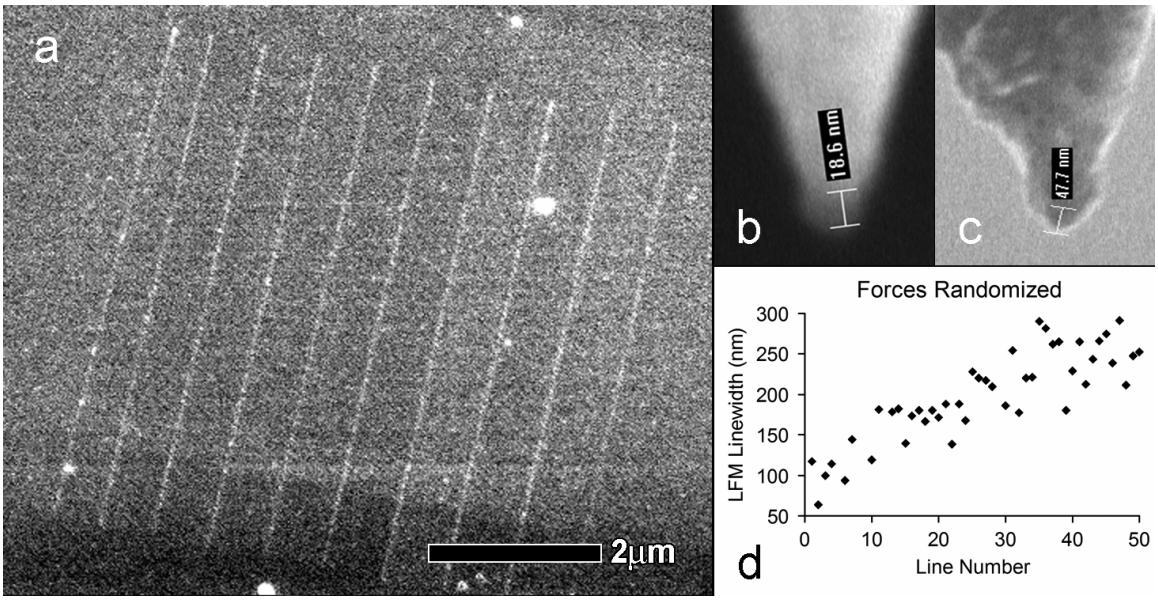

Figure 22. (a) SEM image of ten lines of 1-octadecene chemomechanically functionalized on Si(111)-H at different forces. SEM images of a nitride-coated AFM tip before (b) and after (c) use for chemomechanical functionalization. (d) Graph of linewidth (measured by LFM) vs. order of 50 lines chemomechanically functionalized on silicon with the same tip. Ten forces between 1 and 15 μN were applied in random order for each series of ten lines. Reprinted with permission from Michael V. Lee, Melinda Tonks Hoffman, Katherine Barnett, John-Mark Geiss, Vincent S. Smentkowski, Matthew R. Linford, and Robert C. Davis "Chemomechanical Nanolithography: Nanografting on Silicon and Factors Impacting Linewidth" *Journal of Nanoscience and Nanotechnology* **6**, 1639-1643 (2006). [doi: 10.1166/jnn.2006.220] Copyright © 2006 American Scientific Publishers, http://www.aspbs.com.

Conclusion

We have extended chemomechanical functionalization of silicon by AFM to include nanografting. Alkenes, alcohols, and alkyl halides were nanografted to an alkyl-passivated or alcohol-passivated silicon surface through a chemomechanical process; AFM, SEM, and TOF-SIMS were used to confirm the attachment. Multiple patterning steps with different chemical species were performed and this process was used to demonstrate the ability to "rewrite" the chemical functionalization of a region. Linewidth studies showed that tip wear is a significant issue when writing with Si_3N_4 coated AFM probes. Harder tips, such as diamond or possibly single crystal Si_3N_4 with a constant

radius of curvature are expected to show a stronger correlation between force and linewidth.

Attribution

This work was joint effort between both the Linford and Davis groups. Dr. Robert Davis provided the AFM and image analysis software. Melinda Tonks Hoffman performed preliminary experiments and provided training for Katherine Barnett and myself. Melinda Tonks Hoffman and Katherine Barnett performed the experiments evaluating tip wear and provided the SEM images, forces, order, and linewidth data for my analysis. I prepared the monolayers for the nanografting experiments and with some help from John-Mark Geiss, nanografted the layers. I collected the AFM nanografting data. I collected the TOF-SIMS data and performed the univariate analyses. Dr. Vincent Smentkowski provided the AXSIA analysis and derivative images and spectra.

---

[1] Linford, M. R.; United States Patent No. 6,132,801; 2000.

[2] Niederhauser, T. L.; Jiang, G.; Lua, Y.-Y.; Dorff, M. J.; Woolley, A. T.; Asplund, M. C.; Berges, D. A.; Linford, M. R. *Langmuir* **2001**, *17*, 5889.

[3] Niederhauser, T. L.; Lua, Y.-Y.; Jiang, G.; Davis, S. D.; Matheson, R.; Hess, D. A.; Mowat, I. A.; Linford, M. R. *Angew. Chem., Int. Ed. Engl.* **2002**, *13*, 2353.

[4] Lua, Y.-Y.; Fillmore, W. J. J.; Linford, M. R. *Appl. Surf. Sci.* **2004**, *231-232*, 323.

[5] Niederhauser, T. L.; Lua, Y.-Y.; Sun, Y.; Jiang, G.; Strossman, G. S.; Pianetta, P.; Linford, M. R. *Chemistry of Materials* **2002**, *14*, 27.

[6] Lua, Y.-Y.; Lee, M. V.; Fillmore, W. J. J.; Matheson, R.; Sathyapalan, A.; Asplund, M. C.; Fleming, S. A.; Linford, M. R. *Angew. Chem., Int. Ed. Engl.* **2003**, *42*, 4046.

[7] Lua, Y.-Y.; Fillmore, W. J. J.; Yang, L.; Lee, M. V.; Savage, P. B.; Asplund, M. C.; Linford, M. R. *Langmuir* **2005**, *21*, 2093.

[8] Jiang, G.; Niederhauser, T. L.; Fleming, S. A.; Asplund, M. C.; Linford, M. R. *Langmuir* **2004**, *20*, 1772.

[9] Jiang, G.; Niederhauser, T. L.; Davis, S. D.; Lua, Y.-Y.; Cannon, B. R.; Dorff, M. J.; Howell, L. L.; Magleby, S. P.; Linford, M. R. *Colloids and Surfaces A: Physicochemical and Engineering Aspects* **2003**, *226*, 9.

[10] Wacaser, B. A.; Maughan, M. J.; Mowat, I. A.; Niederhauser, T. L.; Linford, M. R.; Davis, R. C. *Appl. Phys. Lett.* **2003**, *82(5)*, 808.

[11] Kramer, S.; Fuierer, R. R.; Gorman, C. B. *Chem. Rev.* **2003**, *103*, 4367.

[12] Hurley, P. T.; Ribbe, A. E.; Buriak, J. M. *J. Am. Chem. Soc.* **2003**, *125*, 11334.

[13] Piner, R. D.; Zhu, J.; Xu, F.; Hong, S.; Mirkin, C. A. *Science* **1999**, *283*, 661.

[14] Liu, M.; Amro, N. A.; Chow, C. S.; Liu, G.-Y. *Nano Letters* **2002**, *2*, 863-867.

[15] Headrick, J. E.; Armstrong, M.; Cratty, J.; Hammond, S.; Sheriff, B. A.; Berrie, C. L. *Langmuir* **2005**, *21*, 4117-4122.

[16] Xu, S.; Liu, G.-Y. *Langmuir* **1997**, *13*, 127-129.

[17] Liu, J.-F.; Cruchon-Dupeyrat, S.; Garno, J. C.; Frommer, J.; Liu, G.-Y. *Nano Letters* **2002**, *2*, 937-940.

[18] Linford, M. R.; Fenter, P.; Eisenberger, P. M.; Chidsey, C. E. D. *J. Am. Chem. Soc.* **1995**, *117*, 3145-3155.

[19] Keenan, M.R.; Kotula, P.G. U.S. Patent 6,584,413, June 24, 2003. Keenan, M.R.; Kotula, P.G. U.S. Patent 6,675,106, Jan 6, 2004.

[20] Ohlhausen, J. A.; Kotula, M. R.; Peebles, D. E. *Appl. Surf. Sci.* **2004**, *231-232*, 230-234.

[21] Smentkowski, V. S.; Ohlhausen,; J. A.; Kotula, P. G.; Keenan, M. R. *Appl. Surf. Sci.* **2004**, *231-232*, 245-249.

[22] Kim, K. H.; Moldovan, N.; Ke, C. H.; Espinosa, H. D.; Xiao, X. C.; Carlisle, J. A.; Auciello, O. *Small* **2005**, *1(8-9)*, 866.

Chapter 5. Nanografting of silanes on silicon dioxide with applications to DNA localization and copper electroless deposition*

Michael V. Lee,[†] Kyle A. Nelson,[‡] Laurie Hutchins,[‡] Hector A. Becerril,[†] Samuel T. Cosby,[‡] Jonathan C. Blood,[‡] Dean R. Wheeler,[‡] Robert C. Davis,[§] Adam T. Woolley,[†] John N. Harb,[‡] Matthew R. Linford[†]

Abstract

We report the first, successful, partial *nanoshaving* of octadecyl- and octyl-dimethylmonochlorosilane monolayers on silicon dioxide, as well as *nanografting* of perfluorinated- and amino- silanes on these substrates, using an atomic force microscopy (AFM) tip. Even partial nanografting of aminosilane patterns can be used for DNA localization or for binding palladium ions to serve as seeds for electroless deposition of copper lines. That is, even the substitution of a small fraction of chemical species at a surface during nanografting primes the surface to allow significant chemical changes to occur in subsequent processing steps. We characterize our surfaces using AFM, X-ray photoelectron spectroscopy, spectroscopic ellipsometry, and contact angle goniometry.

* Reproduced with permission from *Chemistry of Materials* **2007**, Submitted for publication.

[†] Department of Chemistry and Biochemistry

[‡] Department of Chemical Engineering

[§] Department of Physics and Astronomy

Overview

Nanoshaving and nanografting were first introduced in 1997.[1,2] These nanoscale patterning methods have been used in a variety of applications. For example, nanoshaving, which uses an atomic force microscopy (AFM) tip to mechanically remove a molecular monolayer, has been shown to remove sexithiophene crystals physisorbed between electrical contact pads on silicon dioxide,[3] to pattern streptavidin on gold surfaces for DNA binding,[4] and to remove covalently attached alkyl monolayers from a silicon surface.[5] Nanografting is physisorption or chemisorption of a species of interest concurrent with nanoshaving. Nanografting has been used to pattern various thiols on gold,[6] including thiolated-DNA[7] and bifunctional compounds that bind proteins,[8] as well as alkene, alcohol, and alkyl halide monolayers on silicon.[9,10] From a materials science perspective, it is advantageous to be able to nanograft on an insulating surface as shown in this work, in addition to nanografting on metal and semiconductor surfaces, which has already been demonstrated. Silicon dioxide is a desirable substrate for nanografting because it is available as an atomically flat substrate, it can form strong covalent bonds, especially to silanes, and it is inexpensive.

Other scanning probe microscopy (SPM) methods, besides AFM nanografting, have been used to pattern silicon dioxide with certain limitations. For example, SPM electrochemical oxidation of silane layers allows silver and gold metallization, as well as the localization of DNA on silicon dioxide.[11,12,13] Dip-pen nanolithography has been used to deposit aminosilanes which bind gold particles,[14] or alternatively, to deposit proteins.[15]

Two other published reports relate specifically to nanoshaving of silanes, and to this work. One indicated that even with AFM tip forces of 3 μN, octadecyltrichlorosilane

monolayers could not be removed from silicon dioxide.[5] The other, an AFM tribology study of silanes on mica, reported that the strength of silane films is heavily dependent on their cross-linking networks.[2] Elimination of this cross-linking should facilitate nanoshaving of silanes on silicon dioxide. Accordingly, and although previous attempts have been unsuccessful,[5] in this paper we demonstrate at least partial nanoshaving, and also nanografting, of silanes on silicon dioxide. The viability of biological and nanocircuitry applications is also demonstrated.

Experimental

Neat silane monolayer formation

Silicon wafers bearing native or thermally grown silicon dioxide were piranha-cleaned (7 parts conc. H_2SO_4 to 3 parts 30% aqueous H_2O_2) for 10 minutes at 100-130°C; *caution: piranha solution is extremely dangerous and should be handled with great care*) or plasma-cleaned (10-30 seconds on high setting with a PDC-32G instrument from Harrick Plasma, Ithaca, NY) prior to silane application. Wafers were passivated against plating by capping their surface with octyldimethylmonochlorosilane (C_8DMS, Gelest, Morrisville, PA). The passivation step required a wafer to be placed in a clean glass vial and covered with neat C_8DMS. The vial was purged with dry nitrogen, sealed with a septum stopper, and heated to 80ºC for 20 minutes, which is an adaptation of a literature procedure.[16] Anhydrous methanol was then added and the vial was sonicated. The wafer was removed and rinsed with methanol, and finally placed in a new bath of methanol and sonicated again. This sonicating in fresh methanol was repeated a third time. The wafer was then rinsed with methanol and dried with a jet of nitrogen.

Nanoshaving and nanografting

Silane passivated wafers were patterned with an atomic force microscopy (AFM) tip. Alkylsilane-terminated oxide was nanografted by mechanical removal of the C_8DMS layer with an AFM tip in the presence of another silane. All AFM patterning and imaging was performed with a Dimension 3100 AFM with a fluid cell (Digital Instruments, Santa Barbara, CA) using high-k Si_3N_4-coated silicon cantilevers (NSC11/Si3N4/AlBS, Mikromasch, Estonia). Forces on the order of 10 μN were applied to remove the alkylsilane passivating layers. After nanografting, the samples were removed from the AFM and put in a vial of clean, anhydrous, spectrograde methanol and sonicated for two minutes. The wafer was removed and put in another vial with fresh methanol and sonicated. This was repeated a third time and the sample was blown dry with particle free nitrogen. Following nanografting with APDES and after sonication in methanol the surface in Figure 28 was brushed gently with an aqueous 2 wt. % soln. of sodium dodecylsulfate; it was then rinsed with Millipore water and blown dry with a gentle flow of nitrogen.

DNA treatment

The solution of λ-DNA was 10 ng/μL in TE buffer. The TE buffer was 10 mM Tris and 1mM EDTA in ultrapure water (Millipore) with pH adjusted to 7.2 using NaOH. After aminopropymethyldiethoxysilane (APDES) treated wafers were exposed to this solution for 10 min, they were rinsed with ultrapure water and dried.

Plating chemistry

A three-step process was followed to provide uniform plating on the amine-terminated surfaces. Surfaces were first exposed for 5 minutes to an acidic palladium chloride solution (10 mg $PdCl_2$ in 100 mL Millipore water plus 10 drops of 37% HCl) diluted 10-fold in water. Then they were placed in a solution of 0.15g $NaBH_4$ in 25 mL of Millipore water for 30 seconds to reduce the Pd^{2+} to Pd. After palladium seeding, the surfaces were immersed in an electroless plating solution (3g $CuSO_4$, 14g potassium sodium tartrate, 4g NaOH, and 200mL H_2O; combined 80:1 with 37% formaldehyde in water just prior to plating).[17]

Spectroscopic ellipsometery

Ellipsometry measurements were taken with an M-2000D spectroscopic ellipsometer from the J. A. Woollam Company. All measurements were taken at an angle of incidence of 75° with the full wavelength range (190 to 1000 nm). The data were modeled using the optical constants provided with the instrument software for silicon (si_jaw.mat) and silicon dioxide (sio2_jaw.mat). The silicon dioxide model was used to estimate the layer thickness for the silane layers as well as for the silicon dioxide layers.

Contact angle goniometry

Advancing water contact angles for each surface are reported as the average of measured angles from both sides of a drop on each of 3-4 samples. The angles were measured using a Ramé-Hart model 100-00 goniometer.

X-ray photoelectron spectroscopy (XPS)

Surfaces were characterized by XPS (ESCA SSX-100, Surface Science) throughout the patterning and plating procedure. Monochromatized Al Kα X-rays (1486 eV) were used. The instrument employs a hemispherical analyzer with a take-off angle of 52° from normal. The latest version of the instrument software (ESCA 2005 B v5.01, Service Physics, Bend, OR) was used for data acquisition and analysis.

Process characterization

Plating chemistry

Because it is possible to more thoroughly characterize planar surfaces than nanoscale features on surfaces, the chemistry reported in the work was validated on planar surfaces before being applied to nanoscale patterns. Accordingly, both C_8DMS-terminated silicon and bare silicon dioxide shards were placed in vials, covered with APDES, purged with dry nitrogen, and sealed with a septum stopper. After an hour of incubation at room temperature, dry methanol was added to the vials by needle through the septum (typically about 4-8mL). Samples were then sonicated inside their vials for 2 minutes. Vials were next opened and wafers were removed and sonicated in clean, dry methanol for 2 minutes. Wafers were then dried with nitrogen. Next, these wafers were seeded with Pd^{2+} and plating was attempted using the same procedure employed in the nanografting experiments. XPS measurements were taken for samples at each step in the process: the initial C_8DMS or oxide surface (initial), after application of APDES (APDES), and after copper plating (Cu). The resulting XPS ratios to silicon of carbon, nitrogen, palladium, and copper are presented in Figure 23.

As expected, there is an increase in carbon and nitrogen with the application of APDES to clean oxide samples, but no such increases are observed for the C_8DMS treated samples. In addition, the only samples that show palladium and copper are the clean oxide samples that have been exposed to APDES and taken through the plating process. The increase in C/Si ratio from APDES application to metal plating for the clean oxide samples is likely adventitious carbon depositing on the relatively high free-energy APDES surface; this increase is not observed on the C_8DMS surfaces where the APDES did not deposit. Palladium and copper were only observed on the oxide samples where the APDES deposited; this leads to the observed attenuation of the N/Si signal after plating on the oxide samples.

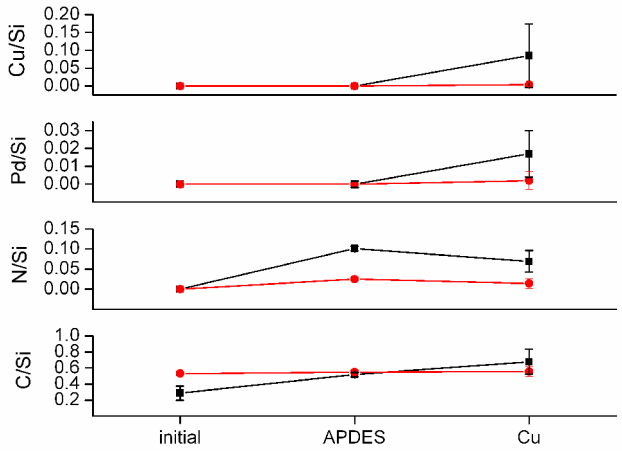

Figure 23. XPS of octyl and oxide surfaces during patterning. Ratios to silicon for carbon, nitrogen, palladium, and copper obtained by XPS. Red indicates samples passivated with a layer of C_8DMS, while black indicates oxide samples at each step of the process. Error bars represent the standard deviation for the samples measured.

The plating solutions were found to change over time. Increased amounts of palladium were found with older solutions, likely due to aggregation of the palladium. The copper electroless solution also degraded over time even without addition of the reducing agent; for optimal results solutions needed to be used within a week of preparation. The large

standard deviations for palladium and copper on the plated samples are representative of the variation obtained with different solutions.

Table 2 shows the layer thicknesses and advancing water contact angles for each successive surface treatment. The C_8DMS layer is comparable to the thickness of a layer of an eight carbon, alkene-terminated monochlorosilane that was previously reported.[16] XPS and the contact angle measurements suggest that there is no significant deposition of APDES on a C_8-passivated silicon dioxide surface.

Table 2. Ellipsometric thicknesses and advancing water contact angles with standard deviations for clean silicon dioxide surfaces, silicon dioxide coated with C_8DMS, silicon dioxide coated with APDES, and C_8DMS coated oxide surfaces treated with APDES.

	Initial		APDES treated	
	Thickness (Å)	θ_{adv}	Thickness (Å)	θ_{adv}
Native SiO_2	18.1 ± 3.3	completely wet	7.0 ± 2.2[(a)]	61 ± 3
[(a)]C_8DMS	7.6 ± 1.2	98 ± 2	0.0 ± 1.9[(b)]	95 ± 3

(a) The thickness of the underlying oxide was subtracted from the total measured thickness.
(b) The thickness prior to application of APDES was subtracted from the value measured after application.

Plating on nanografted lines

Non-specific plating and/or plating outside of the line, which had nucleated at patterned features, was generally observed. Any plating that was observed outside of the lines tended to consist of material that was weakly bound to the substrate and was brushed away by the scanning of the AFM tip in contact mode.

Results and discussion

Nanoshaving on silicon dioxide

Even though others could not nanoshave tri-functional, highly cross-linked octadecyltrichlorosilane monolayers, we were able to partially nanoshave the monochloro analog, octadecyldimethylmonochlorosilane (C_{18}DMS),[16] as shown in Figure 24. Such monofunctional silanes should be tethered to the surface by only a single Si-O bond. Typically, we removed 2-4 Å of the layer with a single pass of the AFM tip and more with additional passes. As measured by spectroscopic ellipsometry, the thickness of the C_{18}DMS layers was 9-10 Å, which is comparable to published values for layers of C_{18}DMS deposited by the same method.[16]

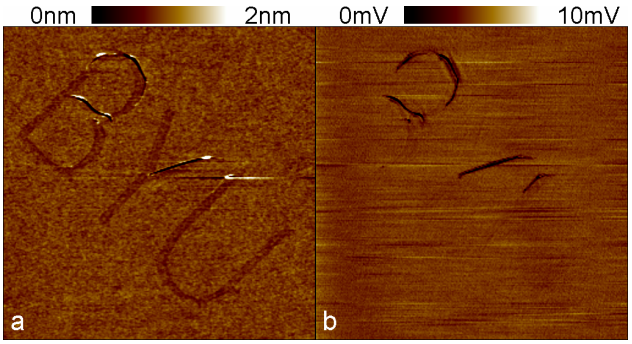

Figure 24. AFM height (a) and lateral force (b) images of the letters "BYU" nanoshaved in a surface of C_{18}DMS on silicon dioxide. The imaged area is 5 μm on a side. The letters are indented approximately 2-4 Å except the deep regions on the top and middle of the "B" and the right arm of the "Y," which show a depth of 1-2 nm. A force of approximately 30 μN was applied to nanoshave these letters.

The letters in Figure 24a show an average depth of 2 Å by AFM, except the regions at the top and middle of the "B" and on the right arm of the "Y." These points of elevated pressure on the surface during nanoshaving (mostly at curved features) led to gouging into the underlying oxide, which demonstrates that although partial nanoshaving is routine, complete nanoshaving should also be possible. It is significant that the partially nanoshaved portions of the "BYU" are nearly invisible in the friction image. The implication of this similarity in lateral force is that the chemistry for the letters remains

essentially identical to that of the background, *i.e.*, composed of methylene (-CH_2-) units. This retention of surface chemistry, together with previous unsuccessful attempts to nanoshave trifunctional silane molecules, suggests that the movement of the tip across the monolayer at high pressure pulls individual molecules out of the monolayer by breaking Si-O bonds rather than Si-C bonds. While the forces used in these experiments are higher than those reported previously,[5] the tips were observed to dull quickly during nanoshaving and nanografting, reducing the effective pressure applied to the monolayer, where the key parameter for nanografting is pressure, not force. Tip dulling was reported previously in a study of chemomechanical nanografting on hydrogen-terminated silicon.[9] Although only a portion of the silane layer is typically removed in this study with a single pass of the AFM tip, it will be shown herein that this removal of silane molecules and the apparent exposure of surface silanol groups for reaction, effectively enables nanografting on silicon dioxide.

Nanografting on silicon dioxide

Even with only partial removal and replacement of the alkylsilane monolayer by nanografting, the surface chemistry is significantly altered. We were able to nanograft both perfluorinated silanes[18] and an aminosilane (APDES)[19] in both C_{18}DMS and C_8DMS monolayers. Accordingly, we present perfluorinated silane lines nanografted in a C_{18}DMS monolayer (Figure 25) and APDES lines nanografted in a C_8DMS monolayer (Figure 26).

The presence of another silane should solvate and facilitate displacement of the alkylsilane molecules that are removed during nanoshaving. The depressions where nanografting was performed are consistent with partial removal of the monolayer and

nanografting of molecules. Because of insertion of the nanografted molecules, the lines are shallower than those seen in Figure 24b. However, the change in the lateral force is unmistakable for the perfluorinated silane (Figure 25b) and even greater with the APDES nanografted lines (Figure 26b). These images differ substantially from the nearly complete absence of contrast in the lateral force image (Figure 24b) for nanoshaving alone. Thus, even though only a portion of the monolayer appears to have been replaced, the surface chemistry still appears to have been transformed. As a further confirmation of the significance of this change, APDES patterns nanografted in a C_8DMS monolayer were used to pattern DNA and also metal.

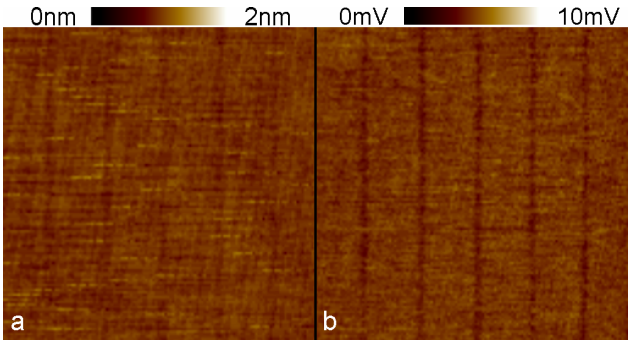

Figure 25. Lines of perfluorinated silane nanografted to silicon dioxide through C_{18}DMS. Panel (a) is AFM height, while (b) is the corresponding lateral force image. Panels (a) and (b) are 2.5 μm on a side. A force of *ca.* 12 μN was applied to the tip during nanografting. The depth of the lines is 0.5 – 1 Å. The linewidths are 100 – 150 nm.

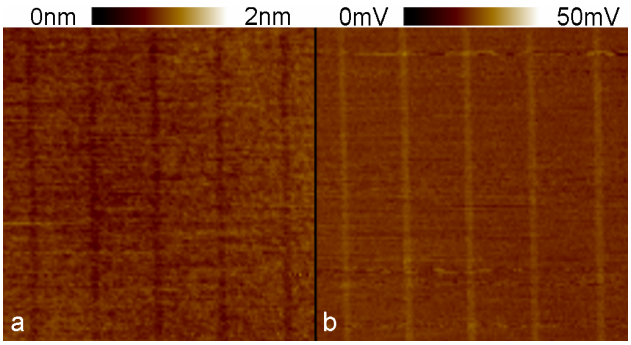

Figure 26. Lines of aminosilane nanografted to silicon dioxide through C_8DMS. Panel (a) is AFM height, while (b) is the corresponding lateral force image. Panels (a) and (b) are 5μm on a side. A force on the order of 60 μN was applied to the tip to nanograft the lines. The depth of the lines is 1 – 1.5 Å. The linewidths are 150 – 200 nm. The contrast in this lateral force image is opposite that in Figure 24 and Figure 25.

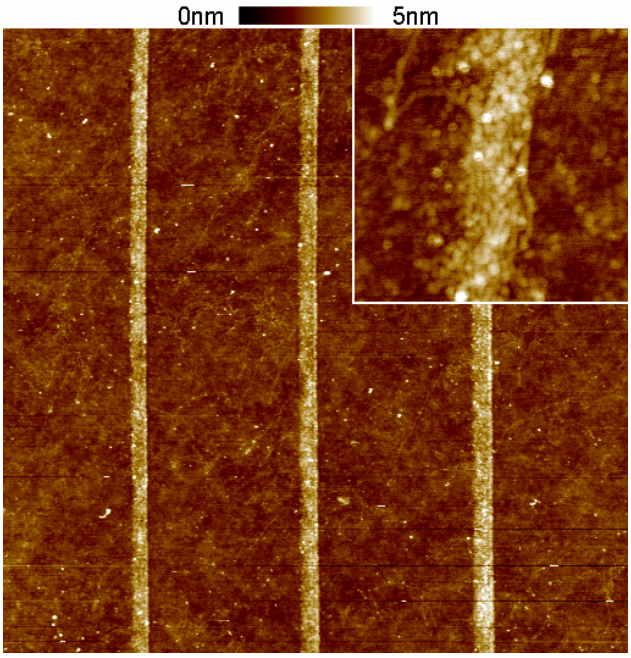

Figure 27. AFM height images of DNA self-aligned on APDES lines nanografted on a C_8DMS monolayer on silicon dioxide. Prior to DNA exposure the lines were depressed, but after exposure, they are *ca.* 3nm tall. The negatively charged DNA ropes deposited preferentially on the positively charged amine-functionalized lines (bright regions). The lines are approximately 100 nm wide. The image is 3 μm on a side. The inset shows a close up image revealing individual DNA strands; the inset is 300 nm on a side.

DNA localization on nanografted aminosilane on silicon dioxide

To create a pattern for localization of DNA, a layer of C_8DMS was nanografted with APDES. The resulting lines showed the characteristic indentation seen before in the AFM height image and the distinct chemical change observed previously by lateral force microscopy. This surface was then exposed to a solution of λ-DNA. The negatively charged DNA molecules associate with positively charged amine groups, but not with the uncharged alkyl layer or with any exposed, negatively charged oxide. Prior to DNA exposure, the patterned areas were lower in height than the surrounding C_8DMS layer, but afterwards, the areas are raised, where ropes of DNA molecules (Figure 27) and individual DNA strands are apparent on and around the lines that were imaged at high lateral resolution (Figure 27 inset). In summary, DNA localization on the patterns illustrates that even if a single nanografting pass doesn't completely replace the alkyl

monolayer with an amine-terminated layer, the exchange of molecules by partial nanografting still results in a significant and useful change in surface chemistry.

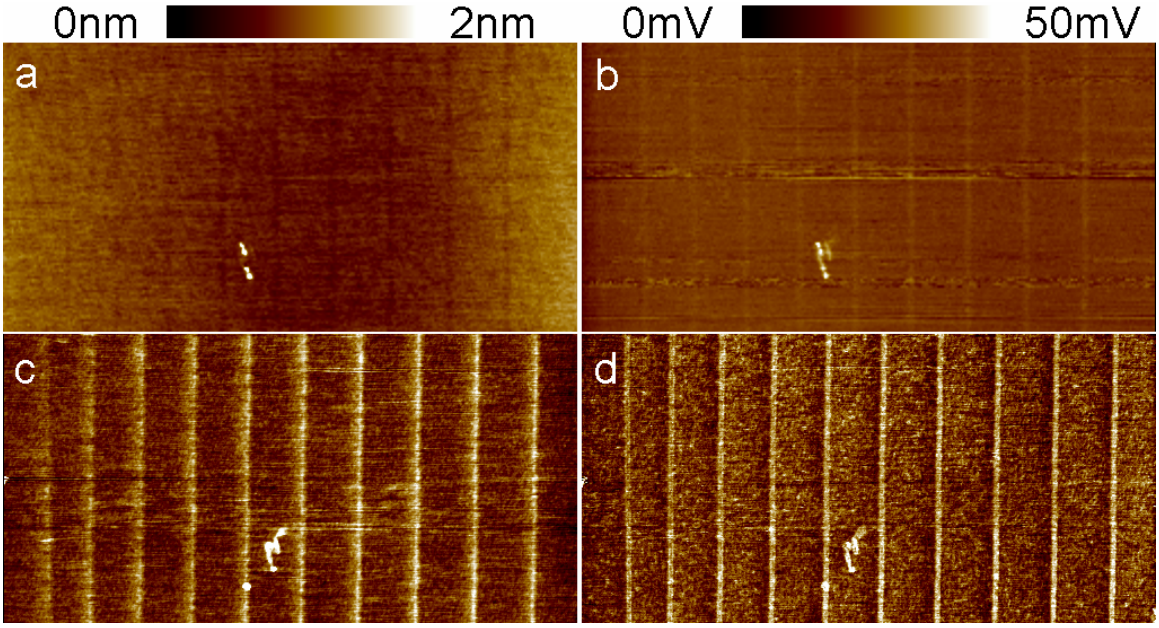

Figure 28. Lines of APDES nanografted through an octyldimethylmonochlorosilane monolayer on silicon dioxide. Panels (a) and (c) are AFM topography images; panels (b) and (d) are lateral force images. Each panel shows a 10 μm x 5 μm region. Panels (a) and (b) were obtained *in situ*, immediately after patterning with APDES. The height image shows an average depression of 0.2 to 0.9 Å for each line, respectively, from left to right, that correlates well with the force used in nanografting, increasing from 9 μN up to 30 μN. The lines show a definite chemical change in panel (b). (The contrast in these lateral force images is opposite to that found in Figure 24 and Figure 25.) The linewidths are *ca.* 200 nm. Panels (c) and (d) were imaged in air subsequent to copper plating. After plating the lines are raised with heights of 2 to 8 Å, from left to right.

Metallization of aminosilane nanografted patterns on silicon dioxide

A principal advantage of using silicon dioxide as a substrate is its dielectric character, which can isolate metal traces on its surface. Because nanografting can create patterns next to objects already on a surface, nanografting on an insulator should be optimal for drawing wires from microscale electrodes to nanoscale objects that cannot be precisely positioned. Feasibility is demonstrated by plating nanografted APDES with an electroless plating scheme: seeding with Pd^{2+}, reduction, and electroless plating with copper.[17] The resulting patterns are shown in Figure 28 and again attest to a change in surface chemistry and topography by nanografting. Panels (a) and (b) in Figure 28, height and

lateral force images, respectively, show the characteristic depression and change in lateral force due to amine nanografting prior to plating. Panels (c) and (d), show raised copper deposition only on the lines, as well as a chemical change on the surface that is much greater than that seen in panel (b). Although the copper as shown is only *ca.* 1nm thick and likely oxidized, a longer plating time or a more inert metal could produce conductive, metallic wires.

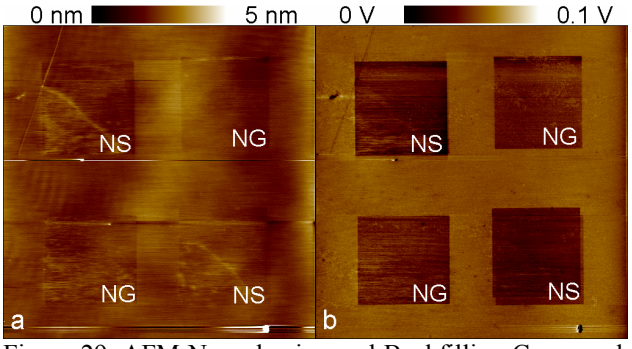

Figure 29. AFM Nanoshaving and Backfilling Compared to Nanografting. Panel (a) is AFM height, while (b) is the corresponding lateral force image. Panels (a) and (b) are 70μm on a side. The initial surface layer was C_{18}DMS. Two boxes, labeled "NS" were nanoshaved into the C_{18}DMS with multiple passes at about 23 μN. Then perfluorinated silane was added and the other two boxes were nanografted, labeled "NG," with a force of 26 μN. The images were then taken with a low-k AFM tip. All four boxes show a small decrease in height of the layer and a similar contrast change. The image was taken in air after removal of the perfluorinated silane and cleaning and drying the surface.

Backfilling nanoshaved areas on silicon dioxide

In addition to showing the feasibility of nanografting on monochlorosilane monolayers, we were also interested in the possibility of nanoshaving in the air and then backfilling the exposed region with a silane, analogous to that demonstrated with thiols on gold.[20] To achieve this, we nanshaved two boxes (labeled NS in Figure 29) with multiple passes of the tip and then wetted this surface with the perfluorosilane. Two additional boxes were then nanografted with a single pass of the tip (labeled NG in Figure 29). As the tip moves over the surface to functionalize the area within the box by drawing closely spaced lines, the overlap between successive lines is a likely source of the apparent increased contrast

compared to that seen in Figure 25b, which is approximately an order of magnitude lower. The similarity between the surfaces with both backfilling and nanografting suggests that individual silane molecules from the initial surface are indeed removed and replaced by the second silane.

Conclusion

We have demonstrated at least partial nanoshaving as well as nanografting of various silanes on silicon dioxide. Both octadecyl- and octyl- dimethylmonochlorosilane monolayers were removed and patterns were made by nanografting both perfluorinated silanes and aminosilanes. DNA was localized on aminosilanes and individual strands were imaged. Pd^{2+} was also allowed to associate with aminosilane lines and electroless plating was demonstrated. This method should allow conductive wires to be drawn to test electrical properties of nanoscale objects on surfaces.

Attribution

Kyle Nelson, Laurie Hutchins, Samuel Cosby, and Jonathan Blood performed the macroscale characterization of samples including preparation of the electroless copper deposition solutions with direction from myself. I collected the XPS data with some assistance from Kyle Nelson and Laurie Hutchins. Dr. Hector Becerril and Dr. Adam Woolley provided expertise in nanoscale patterning, especially with DNA. Dr. Hector Becerril and Kyle Nelson provided the DNA localization data. Dr. Robert Davis provided the AFM for all experiments, except the DNA localization, as well as expertise in nanopatterning and AFM operation and data interpretation. Dr. John Harb and Dr. Dean Wheeler provided metallization expertise. Dr. Matthew Linford provided vital expertise

with silanes and surface patterning. Dr. John Harb provided organization to the group. I prepared the nanoshaving and nanografting samples shown with assistance from Kyle Nelson. With input from all members of the group I prepared the final analysis of the work presented in this chapter.

---

[1] Xu, S.; Liu, G.-Y. Langmuir 1997, 13, 127-129.

[2] Xiao, X.-D.; Liu, G.-Y.; Charych, D. H.; Salmeron, M. Langmuir 1995, 11, 1600-1604.

[3] Chwang, A. B.; Granstrom, E. L.; Frisbie, C. D. Advanced Materials 2000, 12, 285-288.

[4] Zhou, D.; Bruckbauer, A.; Ying, L.; Abell, C.; Klenerman, D. *NanoLett.* **2003**, *3*, 1517-1520.

[5] Headrick, J. E.; Armstrong, M.; Cratty, J.; Hammond, S.; Sheriff, B. A.; Berrie, C. L. *Langmuir* **2005**, *21*, 4117-4122.

[6] Xu, S.; Miller, S.; Laibinis, P. E.; Liu, G.-Y. *Langmuir* **1999**, *15*, 7244-7251.

[7] Liu, M.; Amro, N. A.; Chow, C. S.; Liu, G.-Y. *NanoLett.* **2002**, *2*, 863-867.

[8] Zhou, D.; Wang, X.; Birch, L.; Rayment, T.; Abell, C. *Langmuir* **2003**, *19*, 10557-10562.

[9] Lee, M. V.; Hoffmann, M. T.; Barnett, K.; Geiss, J.-M.; Smentkowski, V. S.; Linford, M. R.; Davis, R. C. *Journal of Nanoscience and Nanotechnology* **2006**, *6*, 1639-1643.

[10] Yang, L.; Lua, Y.-Y.; Lee, M. V.; Linford, M. R. *Acc. Chem. Res.* **2005**, *38*, 933-942.

[11] Moaz, R.; Frydman, E.; Cohen, S. R.; Sagiv, J. *Adv. Mater.* **2000**, *12*, 424-429.

[12] Liu, S.; Maoz, R.; Schmid, G.; Sagiv, J. *NanoLett.* **2002**, *2*, 1055-1060.

[13] Shin, M.; Kwon, C.; Kim, S. K.; Kim, H. J.; Roh, Y.; Hong, B.; Park, J. B.; Lee, H. *NanoLett.* **2006**, *6*, 1334-1338.

[14] Sheu, J.-T.; Wu, C.-H.; Chao, T.-S. *Jap. J. App. Phys.* **2006**, *45*, 3693-3697.

[15] Lim, J.-H.; Ginger, D. S.; Lee, K.-B.; Heo, J.; Nam, J.-M.; Mirkin, C. A. *Angew. Chem. Int. Ed.* **2003**, *42*, 2309-2312.

[16] Husseini, G. A.; Peacock, J.; Sathyapalan, A.; Zilch, L. W.; Asplund, M. C.; Sevy, E. T.; Linford, M. R. *Langmuir* **2003**, *19*, 5169-5171.

[17] Gutzeit, G.; Saubestre, E. B.; and Turner, D. R. In *Electroplating Engineering Handbook Third Edition*; Graham, A. K.; Van Nostrand Reinhold Company: New York City, NY, 1971; pp 505.

[18] perfluoroalkylethyltriethoxysilane (predominantly perfluorohexylethyl and perfluorooctylethyl homologs), 90%+, Gelest

[19] 3-aminopropylmethyldiethoxysilane, 95%+, Gelest

[20] Abbott, N. L.; Folkers, J. P.; Whitesides, G. M. *Science* **1992**, *257*, 1380-1384.

Chapter 6. Discussion and future work

Silicon model surface for chemomechanical functionalization

The general model for reactions with scribed silicon has employed the silicon {001} surface, as was used in Chapter 2. The Si(001) plane is one of the thermodynamically favored planes. When bare in vacuum, this surface reconstructs to form dimers between adjacent silicon atoms. Because the double bond in the silicon dimer is relatively weak, 5-10 kcal/mol,[1,2,3] it often acts like two single radicals. The reaction of a dimer with unsaturated hydrocarbons like 1-alkenes and 1-alkynes, however, forms a four-member ring similar to that resulting from a [2+2] cycloaddition. Other reagents used in chemomechanical functionalization like alcohols, epoxides, and amines, bind through a single covalent bond. Monolayers of these molecules will not have the same restrictions and patterns as found in Chapter 2 and will be better represented by simulations on silicon surfaces with molecules bound to only a single silicon atom.[4,5]

When the surface is scribed in chemomechanical functionalization, the resulting surface is rough on the order of nanometers or microns, for AFM or macroscale functionalization, respectively. The unit cell for silicon is Fd-3m and about 0.5 nm on a side, which means that each 0.5 nm of depth goes through four layers of silicon atoms. If silicon with nanometer roughness from scribing with a tungsten carbide ball or an AFM tip were to be annealed, the surface would likely be able to revert to a smoother surface; however, without annealing, it is likely that a disordered surface is created. The disruption of the surface with macroscale scribing is even greater. It is interesting to note that although the surfaces have a great deal of roughness, in Figures 17 and 18 in Chapter 3, the peak visible above the rising baseline is at the desorption temperature for

molecules bound by two Si-C bonds. This indicates that the principal binding of the molecules is via two bonds rather than just one. Even though the surface is rough on the micron scale, the structure of the rough surface is close enough to Si(001)-2x1 reconstruction to allow di-σ binding. This confirms the applicability of using this model for scribed silicon surfaces.

The desorption temperatures for acetylene reacted in a [2+2] cycloaddition-like reaction with a Si(001)-2x1 dimer or reacted with a rest atom and adatom in the Si(111)-7x7 reconstructed surface are nearly the same.[6,7,8,9,10,11,12,13] This indicates that although the di-σ binding of the acetylene and ethylene to the silicon surface is supported and acetylene reacts with the radical scribed surface similarly to the reaction with Si(001)-2x1 and Si(111)-7x7, the actual nature of the surface is still ambiguous. The broader range of binding energies for di-σ bound molecules indicated by the broad thermal desorption spectroscopy (TDS) spectra peaks for the chemomechanically functionalized samples does confirm that the surface after mechanical abrasion is not a perfect Si(001) or Si(111) surface.

Comparison and calibration

Ethylene and acetylene have been intensely studied on the Si(001)-2x1 and Si(111)-7x7 surfaces. The methods used to experimentally determine and confirm the binding on these surfaces could be applied to silicon scribed in the presence of acetylene and ethylene. Methods like high resolution electron energy loss spectroscopy (HREELS) and auger electron spectroscopy (AES),[14,15,16] laser induced thermal desorption,[17,18] scanning-tunneling microscopy,[19,20] have been used to analyze the binding of ethylene and acetylene with silicon surfaces. These same methods could be performed on samples

scribed with ethylene or acetylene in air, scratched in vacuum or inert atmosphere and then dosed in UHV with acetylene or ethylene, or dosed with acetylene or ethylene after heating to desorb oxygen in UHV. These experiments would provide better understanding of the silicon surface produced during chemomechanical functionalization.

After saturating Si(001) or Si(111) in UHV with ethylene or acetylene, barring surface defects, complete coverage is expected. The ability of these layers to passivate the silicon surface could be evaluated by taking such samples out of UHV and analyzing them by XPS and TOF-SIMS. 10-10000 Langmuir will saturate a bare silicon surface in UHV at room temperature,[15,21] which takes less than 20 μs in acetylene or ethylene at atmospheric pressure. The amount of oxidation on surfaces originally prepared in UHV and then exposed to atmospheric oxygen could be compared with that found for surfaces scribed in the presence of these gases; although the experiments in Chapter 3 may need to be repeated and oxygen completely excluded during chemomechanical functionalization. Comparison of results for scribed silicon with surfaces dosed in UHV provides calibration to determine completeness of coverage during chemomechanical functionalization with gases.

An important ability with patterning methods is quickly switching between various molecules. Because chemomechanical or nanografting methods will deposit whatever reactive molecule is present, using a flow cell and changing the reactant during scribing allows functionalization with many different molecules on the same sample without removing the sample. Using gases or a reactive molecule in an inert solvent can make the transition even more cleanly and quickly. Gases are cleaner, but the solvent can also suspend particles that are produced and help remove them. A valuable study to show the

versatility of chemomechanical methods would be to functionalize three different areas with three different molecules without changing the sample or tip by using a sealed flowcell to provide the functional molecules to be patterned.

The comparative reaction rates with different molecules could also be compared by providing a mixed atmosphere of reactive molecules each with a characteristic heteroatom. The ratio of the two could be varied for different scribed samples. XPS could determine the percent composition of each monolayer for each combination of reactive groups. This could be used to determine relative reaction rates. If control can be achieved by changing concentrations, monolayer composition could be adjusted by *in situ* regulation of concentration rather than completely replacing the reactive solution.

The areas of the roughened surface that transition between different crystal faces will be more accessible for reaction, but would also be more susceptible to oxidation following functionalization. These intersections between crystal faces may be the source of additional oxidation on chemomechanically functionalized samples. The roughness of the surface also limits the size of each planar region, so edge effects are enhanced. Near edges, the monolayers will be less uniform and less resistant to oxidation. This enhanced oxidation is seen in the AXSIA analysis of the TOF-SIMS spectra for the nanografted boxes in Chapter 4, Figure 20. The box shows additional oxygen ions compared with the background. The increased oxygen signal is either from areas that were not functionalized with the perfluorinated species or were attacked by oxygen after functionalization.

Considerations for tip wear

Tip wear due to abrasion by the silicon surface is important to all forms of mechanically-driven AFM nanopatterning methods. The chemomechanical functionalization study on silicon in Chapter 4 shows greater correlation coefficients between the order of line scribing and linewidth than is found for applied force and linewidth. This clearly shows that the tip wear has a significantly greater impact on the linewidth than the applied force does, and is likely the most important factor during chemomechanical functionalization on silicon. Wear is exaggerated on harder surfaces like silicon dioxide. Tip wear limits the area that can be functionalized by a single tip and increases materials costs. This effect limits chemomechanical functionalization to experimental purposes.

The direct contact of an AFM probe tip with a hard surface causes wearing of the tip. Tip wear for nanografting may be mitigated by the passivating layer on the surface. As seen in Chapter 5, an alkyl passivating surface can reduce the friction between the tip and the surface. Because only a portion of the underlying layer was removed in the partial nanografting of silanes on silicon dioxide, the contact between the tip and the surface was lessened, if not completely prevented. Although wear studies were not performed with silane surfaces on silicon dioxide, these surfaces that allow only partial nanografting may demonstrate greater correlation between force and linewidth than was observed with chemomechanical functionalization on hydrogen-terminated silicon.

Utilization of harder AFM probe tips, such as diamond, diamond-coated, or solid silicon nitride, would improve the precision of mechanically-driven AFM methods. Harder tips would at least be less susceptible to wear and may not wear at all. Some have shown diamond tips to be able to repeatedly scribe silicon dioxide without an increase in

feature size. This would also allow characterization and control of the relationship between tip pressure and feature size on silicon or silicon dioxide. Reliable penetration of silicon dioxide without wear effects would also enable complete nanografting of silanes on silicon dioxide.

In order to avoid the complications due to tip wear encountered when performing chemomechanical functionalization, a surface with a monolayer could be formed of molecules with at least one bond significantly weaker than the C-C, Si-O, or Si-C bonds that are formed in the nanografting works presented here. When disturbed with an AFM tip, the bond would be broken and create a reactive species for subsequent functionalization. The tip would not wear as much, and possibly not at all, thus creating finer features. This new method could retain the abundance of reactive molecules available for chemomechanical methods, not require expensive AFM probes, and allow more reproducible patterning.

Partial nanografting on silicon surfaces

The surfaces created with both the nanografting on silicon and nanografting on silicon dioxide appear quite similar. There is a small height change and a large friction change in AFM. The chemical change in nanografting on silicon is also seen in TOF-SIMS and with SEM. On silicon dioxide, the chemical change is confirmed by localizing DNA and plating. The similarity in the effects suggest the possibility that the same thing is happening in both nanografting experiments, *i.e.*, only partial nanografting was performed on each surface. In order to determine whether partial or complete nanografting was performed on silicon, a longer chain would have to be nanografted through the octyl passivating layer. The greater the increase in height of the patterned

regions compared with the surrounding passivating layer, the more complete the nanografting.

Both nanografting on silicon and on silicon dioxide used similar eight carbon alkyl chains with one point of surface attachment as the passivating layer. These layers should act similarly. If one can be penetrated and the surface reached, then the same would be believable for the other, but if one cannot, then that casts doubt on the penetration of the other. In partial nanografting on silicon dioxide, the only times the layer was clearly completely penetrated on the first pass, the silicon dioxide was also penetrated. This suggests that the passivation layer does indeed reduce the friction between the tip and surface. It appears that in chemomechanical nanografting on silicon dioxide, when the pressure is high enough to compress and shear the underlying silicon dioxide, the layer is removed by penetrating into the underlying substrate as well. This may also be true for nanografting on silicon. The alkyl layers are not crystalline and are able to compress, change orientation, and slide along one another. This may only allow partial nanografting on crystalline surfaces unless the substrate can be affected.

Conclusion

I performed experiments that model the scribed silicon surface and also confirm the model used. I extended chemomechanical functionalization to include gaseous reagents. I have merged AFM chemomechanical functionalization with nanografting and demonstrated nanoscale patterning on both silicon and silicon dioxide surfaces. These experiments expanded the scope of chemomechanical functionalization and nanografting and provide groundwork for further covalent patterning on silicon and silicon dioxide.

AFM chemomechanical functionalization and nanografting are versatile methods with room for application in nanoscale patterning. In nanocircuitry and molecular electronics they can be used to both lay down patterns that can be plated as traces and position molecules for conductive circuits. They can be used to create assays for disease research and detection, genetic studies, or hazardous chemical detection. Hydrophobic/hydrophilic patterns can also be created with these methods to provide guided flow of liquids for lab-on-a chip applications. If chemomechanical patterning can be demonstrated on a polymer, then reactive handles could be patterned on polymers for subsequent polymerizations allowing physical nanostructures to be built with various polymers in a true bottom-up approach. The power of chemomechanical methods lies in creating or placing a functional handle on a surface that otherwise has none.

---

[1] D'Evelyn, M. P.; Cohen, S. M.; Rouchouze, E.; Yang, Y. L. *J. Chem. Phys.* **1993**, *98*, 3560.

[2] Doren, D. J. *Adv. Chem. Phys.* **1996**, *95*, 1.

[3] Lu, X.; Zhu, M.; Wang, X. *J. Phys. Chem. B* **2004**, *108*, 7359-7362.

[4] Sieval, A. B.; van den Hout, B.; Zuilhof, H.; Sudholter, E. J. R. *Langmuir* **2001**, *17*, 2172-2181.

[5] Sieval, A. B.; van den Hout, B.; Zuilhof, H.; Sudholter, E. J. R. *Langmuir* **2000**, *16*, 2987-2990.

[6] Hamers, R. J.; Wang, Y. *Chemical Reviews* **1996**, *96*, 1261.

[7] Buriak, J. M. *Chemical Communications* **1999**, *12*, 1051.

[8] Buriak, J. M. *Chemical Reviews* **2002**, *102*, 1271.

[9] Bent, S. F. *J. Phys. Chem. B* **2002**, *106*, 2830.

[10] Bent, S. F. *Surface Science* **2002**, *500*, 879.

[11] Yoshinobu, J.; Fukushi, D.; Uda, M.; Nomura, E.; Aono, M. *Phys. Rev. B* **1992**, *46*, 9520-9524.

[12] Piancastelli, M. N.; Motta, N.; Sgarlata, A.; Balzarotti A.; De Crescenzi, M. *Phys. Rev. B* **1993**, *48*, 17892–17896.

[13] Zhou, R.-H.; Cao, P.-L.; Lee, L.-Q. *Phys. Rev. B* **1993**, *47*, 10601–10606.

[14] Yoshinobu, J.; Tsuda, H.; Onchi, M.; Nishijima, M. *J. Chem. Phys.* **1987**, *87*, 7332-7340.

[15] Rochet, F.; Jolly, F.; Bournel, F.; Dufour, G.; Sirotti, F.; Cantin, J.-L. *Phys. Rev. B* **1998**, *58*, 11029–11042.

[16] Yi, S. I.; Widdra, W.; Yan, C.; Weinberg, W. H. *J. Vac. Sci. Technol. A* **1996**, *14*, 1822-1825.

[17] Sinniah, K.; Sherman, M. G.; Lewis, L. B.; Weinberg, W. H.; Yates, Jr., J. T.; Janda, K. C. *J. Chem. Phys.* **1990**, *92*, 5700-5711.

[18] Sung, M. M.; Kluth, G. J.; Yauw, O. W.; Maboudian, R. *Langmuir* **1997**, *13*, 6164-6168.

[19] Yoshinobu, J.; Fukushi, D.; Uda, M.; Nomura, E.; Aono, M. *Phys. Rev. B* **1992**, *46*, 9520-9524.

[20] Piancastelli, M. N.; Motta, N.; Sgarlata, A.; Balzarotti, A.; De Crescenzi, M. *Phys. Rev. B* **1993**, *48*, 17892–17896.

[21] Chung, C.-H.; Jung, W.-J.; Lyo, I.-W. *Physical Review Letters* **2006**, *97*, 116102.

Appendix. Analytical methods

Contact angle goniometry

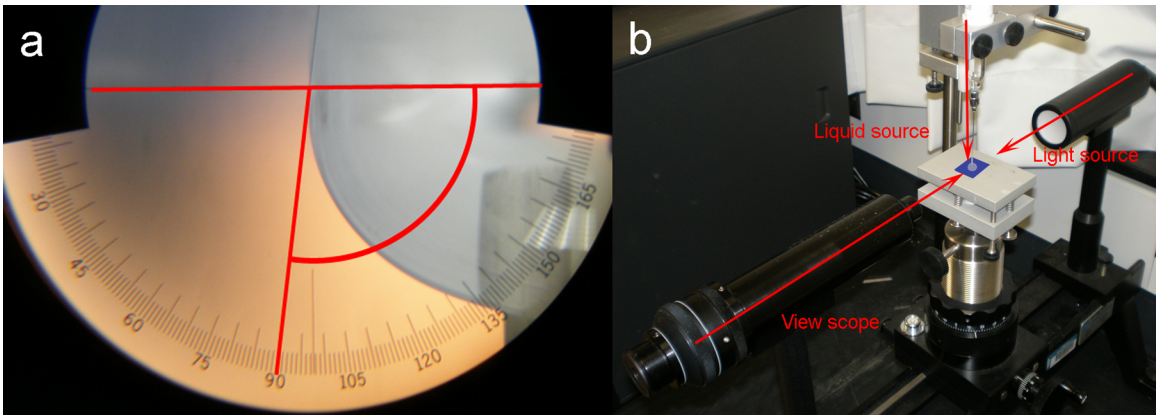

Figure 30. Contact angle goniometry. Panel (a) shows the view through the telescope. The contact angle is measured at the side of the drop, as shown in the image. The image is upside down because of the optics of the instrument. Panel (b) shows the instrument: a syringe with a blunt needle provides the liquid from which a contact angle is measured, the sample is placed on a flat stage that can be raised or lowered, illumination is provided from the back, and the contact angle is measured through a telescope with angle gradations on it.

A contact angle goniometer is an instrument used to measure the contact angle of a liquid with a solid substrate. It consists of a light source, a stage, a liquid dispenser, and a telescope with angle gradations as shown in Figure 30. A sample is placed on a flat stage and then water is dripped onto the surface through a special syringe with a blunt needle. The contact angle is typically measured from the surface, through the drop, and stopping at the drop/air interface, as shown in the image. Contact angle goniometry is used as a measure of the free energy of a surface. For example, a smaller water contact angle indicates a more hydrophilic, higher free-energy surface. If the tip of the needle is positioned so that it is within the drop of water, the volume of the water droplet can be smoothly increased or decreased. If the droplet is increased so that it expands to regions of the sample that have not yet been wetted, the angle at which the water droplet contacts

the surface is called the advancing water contact angle. A rough surface will generally have a greater water contact angle than a similar surface that is smooth.

Spectroscopic ellipsometry

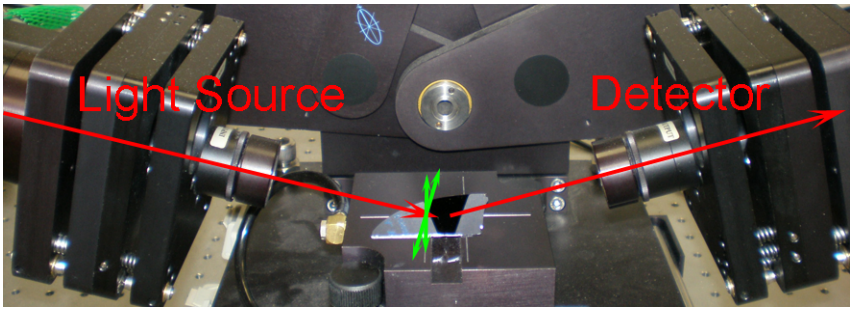

Figure 31. Spectroscopic ellipsometry. In spectroscopic ellipsometry light of wavelengths of interest is directed onto a sample at a designated angle. A detector is aligned to collect the reflected light. Depending on how much of the vertically and horizontally polarized light is captured by the detector, properties or characteristics of the sample, like layer thickness and optical constants, can be determined.

A spectroscopic ellipsometer is an instrument that shines a broad spectrum of wavelengths of light, in our case about 200-1000nm, on a flat sample surface and monitors the light reflected from the surface to determine characteristics of the sample or layers on the sample. The optical constants of the material being measured, and its thickness, determine how the light at each wavelength will interact with the surface. By measuring both the vertical and horizontal polarizations of the light reflected from the surface, the thickness of layers can be determined from their respective optical constants, or vice-versa. Figure 31 shows the typical setup.

X-ray photoelectron spectroscopy

An x-ray photoelectron spectrometer (XPS) irradiates samples of interest with x-rays. In our case, the x-rays are produced by bombarding an aluminum target with a beam of electrons. Core electrons are ejected from aluminum atoms, allowing other electrons to fall down to replace them, and release the excess energy in the form of x-rays. The

monochromatized aluminum K-α line at 1487 eV is one of the most common sources for x-rays for XPS. When these x-rays strike the sample surface, they eject core electrons. When one of these electrons absorbs x-rays from XPS, energy beyond what is required to free the electron from its atom propels the electron in the form of kinetic energy. Because different electrons are bound in different energy levels, the resulting kinetic energy of electrons from different atoms is also different. The kinetic energy of the ejected electrons can be measured to determine the atom from which each originated. The binding environment also modifies the binding energy of electrons, slightly shifting the kinetic energy when ejected. By counting the electrons ejected at each energy level, quantitative elemental composition of the sample can be determined. By monitoring the shifting of these peaks, some insight can be obtained about structure as well as composition of surface species.

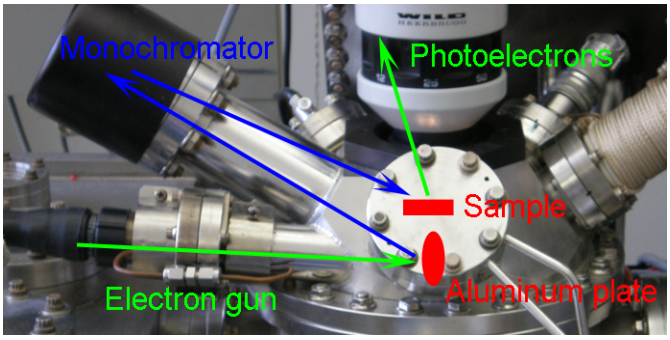

Figure 32. An x-ray photoelectron spectrometer. A beam of high-energy electrons impacting an aluminum target produces x-rays. These x-rays can be monochromatized to irradiate a surface with only a single wavelength, typically the aluminum K-α line. When x-rays irradiate a sample, electrons are ejected that are characteristic of the atom from which they originate. Green lines show electron paths within the spectrometer, while blue lines show x-ray paths. The solid symbols indicate the approximate positions of the sample and aluminum plate within the instrument.

Atomic force microscopy

Atomic force microscopy employs a tip, sharpened to nanometer scale, mounted on a micrometer scale, low-mass cantilever. As this tip is brought close to a surface, small forces on the tip can be measured as deflections of the cantilever. If the tip is scanned

over a surface, the topography of the surface will apply higher (lower) forces to the tip as it scans over raised (recessed) features. If the tip is extended toward and retracted from the surface to maintain a constant force, the extension and retraction can map out the topography of the surface. The AFM is able to probe any surface, conducting or non-conducting, by moving the tip along the surface. This topography mapping is the basis of AFM height measurements.

As the tip is drawn across the surface at constant force in contact mode, which means that the tip remains in contact with the surface during scanning rather than oscillating at its resonant frequency, the interaction between the tip and the surface will change depending on the nature of the surface. This interaction can be termed friction because stronger interactions will exhibit a greater force against the movement of the tip. This friction causes torsion on the cantilever which can be monitored along with height changes. Changes in torsion on the cantilever are indicative of a change in surface chemistry. This is the basis for AFM friction measurements.

Thermal desorption spectroscopy

Heating a sample can reverse an exothermic reaction, which in a simple case breaks a bond. If the bond that is broken was previously holding a molecule to a surface, that molecule can then be captured and analyzed. Such is the case with thermal desorption spectroscopy. Species chemisorbed (or also physisorbed) on a surface can be released from the surface. A more strongly bound species requires more energy to be dislodged; thus, the temperature at which each molecule desorbs is characteristic of the bond strength holding it to the surface. The desorption temperature measurement becomes a

tool for deducing the nature of binding to a surface so long as the molecule of interest does not decompose prior to desorbtion.

Time-of-flight secondary ion mass spectrometry

Mass spectrometers ionize a species of interest and measure the mass-to-charge ratio (m/z) of this species and any fragments produced from it during ionization. The plot of counts (signal) versus m/z for all of the ions produced from a sample is the mass spectrum. In time-of-flight secondary ion mass spectrometry (TOF-SIMS), ions are produced by bombarding a surface with primary ions, which in this work are monoisotopic gallium ions. These secondary ions that are produced are characteristic of the surface being impacted. The time-of-flight tube used to measure the mass provides highly accurate m/z values. If the beam is rastered over a surface, a chemical map of the surface can be produced by plotting the mass spectra, or portions of the mass spectra, that are collected at each point.

Principal components and automated expert spectrum image analyses

Two methods of data reduction for complex data sets are principal components analysis (PCA) and multivariate curve resolution (MCR), which I implemented in the automated expert spectrum image analysis (AXSIA) package. When each is used to analyze arrays of mass spectra that represent either groups of samples or unfolded surface images, each spectrum is treated as a point in multidimensional space with each m/z value representing an axis and the intensity of the peak as the value for the sample on that axis. In PCA as shown in Figure 33a, the mean value for each peak is subtracted from each point, effectively centering the data. A new set of orthogonal axes, each a linear combination of

the original peaks, are chosen. The first is aligned so that it represents the greatest variation in the data, the second, the greatest variation remaining in the data, and so forth. The first axes are able to represent most of the variation in the data, thus reducing the complexity of the data. In AXSIA as shown in Figure 33b, the data are not centered and retain only positive values. A recursive function then finds linear combinations of the peaks that best represent the data presented. The component spectra produced are not required to be orthogonal, as is required in PCA.

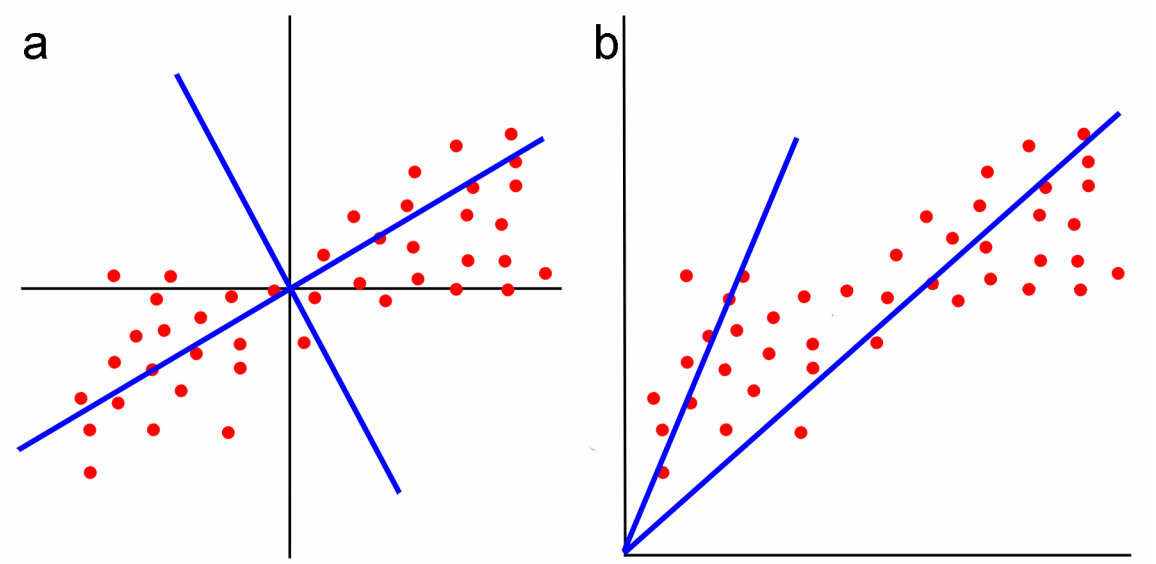

Figure 33. A two-dimensional comparison of PCA and MCR chemometrics analyses. (a) In PCA the data can be imagined as plotted and sometimes centered and then the axes are rotated so that the first axis captures the greatest variation in the data. The second axis is rotated to capture the greatest variation in the data after that accounted for by the first axis. All axis must be orthogonal. (b) In MCR, each spectrum is plotted with each peak represented by one axis. Then an iterative algorithm is applied to find the set of spectra that best represent the variation in the data. These characteristic spectra are not required to be orthogonal.